earth

MDPI

Article

Hydroclimatic Trends, Streamflow Variability, and Land-Use Change in the Ribeira de Iguape River Basin, Brazil

Valéria Machado Emiliano *, Jakeline Baratto, Nádia Gilma Beserra de Lima, Emerson Galvani * and Paulo Miguel de Bodas Terassi

Department of Geography, University of São Paulo (USP), São Paulo 05508-080, Brazil; jakelinebarattogeo@gmail.com (J.B.); nadia.lima@usp.br (N.G.B.d.L.); pmbterassi@usp.br (P.M.d.B.T.)
* Correspondence: valeriamachadoemiliano@usp.br (V.M.E.); egalvani@usp.br (E.G.)

Abstract

Hydroclimatic variability and land-use and land-cover (LULC) change were investigated in the Ribeira de Iguape River Basin, Brazil, using precipitation records from 14 gauges and mean, maximum and minimum streamflow from 10 stations within 1960–2024, alongside annual LULC maps for 1985–2024. Hamed–Rao Mann–Kendall tests, Sen's slopes and change-point analyses were complemented by temporal-dependence, interstation-consistency and false-discovery-rate diagnostics. After adjustment, seven precipitation stations exhibited increasing annual trends and one showed a decrease. The largest positive slopes occurred at Balsa do Cerro Azul (+101.5 mm decade^{-1}), Guanhanha (+98.3 mm decade^{-1}) and Capela da Ribeira (+90.1 mm decade^{-1}). However, pronounced departures from regional reference series around 1981 at two neighbouring gauges preclude an unequivocal climatic interpretation. Streamflow responses were more localised. Declining maximum discharge at Juquiá (-16.2 m^3 s^{-1} decade^{-1}) was the only annual streamflow trend retained after adjustment, without a comparable downstream decline over common years. Urban and mining areas expanded, whereas forest cover initially declined and subsequently recovered partially, remaining below its 1985 extent. Land-cover proportions extracted within ten independently DEM-delineated upstream catchments yielded 228 estimable contemporaneous LULC–discharge correlations. Although 21 were nominally significant, none remained significant after Benjamini–Hochberg adjustment within the corresponding discharge-metric families or across the pooled set. These findings reveal spatially differentiated hydroclimatic and landscape trajectories, without establishing a causal contribution of LULC change to observed streamflow variability.

Keywords: streamflow variability; hydroclimatic trends; land use and land cover change; change-point detection; false discovery rate; Ribeira de Iguape River Basin

Check for updates

Academic Editor: Ashraf Dewan

Received: 17 September 2026
Revised: 30 October 2026
Accepted: 1 November 2026
Published: 5 November 2026

Copyright: © 2026 by the authors. Licensee MDPI, Basel, Switzerland. This article is an open access article distributed under the terms and conditions of the Creative Commons Attribution (CC BY) license.

1. Introduction

Watersheds provide a spatial basis for examining water availability because precipitation, relief, soils, vegetation and human interventions interact within a connected drainage system [1,2]. Their joint influence on runoff generation and routing also links the physical processes of the water balance to water use and environmental management, making the watershed a widely adopted unit for regional assessment [3,4].

Streamflow integrates precipitation inputs, infiltration, soil-water storage, evapotranspiration and surface and subsurface runoff. Historical discharge records therefore permit the assessment of gradual trends and abrupt changes in river regimes, with mean,

maximum and minimum flows representing distinct hydrological responses. Nonparametric trend and change-point methods have been widely applied to estimate the direction, magnitude and timing of these variations [5,6].

Although precipitation is the principal atmospheric input to the water balance, similar rainfall changes can produce different discharge responses where storage, evapotranspiration, water use and landscape characteristics differ among catchments. Brazilian studies have documented precipitation and discharge changes that diverge in timing or magnitude [6–8], while analyses incorporating teleconnections, hydrological persistence and LULC indicate that their correspondence also depends on temporal scale and catchment characteristics [9–14].

Vegetation loss and regeneration, urbanisation, agriculture and mining can modify interception, infiltration, evapotranspiration and runoff pathways [1], but their associations with mean and extreme flows depend on the extent, location and hydrological connectivity of the affected surfaces [7,8,15,16]. Combining discharge records with annual land-cover observations can therefore help distinguish changes that coincide within contributing areas from regional trajectories whose apparent correspondence arises at a different spatial or temporal scale.

Annual MapBiomas maps have substantially extended the temporal coverage of land-use assessment in Brazil since 1985. Applications of these Landsat-based series demonstrate their relevance to regional and catchment analyses [17,18]. Their annual resolution permits the examination of trends, candidate transitions and contemporaneous hydroclimatic associations. Jiang et al. [19] documented concurrent changes in land cover and streamflow whose interpretation depended on climatic and catchment conditions. In the Iguaçu Triple Frontier, Terassi et al. [20] jointly analysed LULC trajectories and climatic indicators, distinguishing statistical correspondence from causal attribution.

The Ribeira de Iguape River Basin combines extensive Atlantic Forest remnants, mangroves and restingas with urban, agricultural and mining activities and areas occupied by traditional communities [21,22]. Differences in elevation, relief and maritime influence contribute to pronounced spatial variability in precipitation and hydrological response. In the estuarine sector, the Valo Grande Canal has altered the hydrosedimentological dynamics of the Cananéia–Iguape system [23]. These environmental contrasts make the basin particularly relevant to the joint assessment of hydroclimatic and landscape change.

Regional assessments integrating precipitation, several discharge metrics and annual LULC trajectories remain limited for the Ribeira de Iguape Basin. Examining these components together can clarify whether their changes coincide over comparable periods and contributing areas, provided that the interpretation accounts for differences in record coverage, spatial support and statistical assumptions rather than treating temporal association as evidence of a shared cause.

This study examines precipitation and mean, maximum and minimum discharge variability in the Ribeira de Iguape River Basin using available observations within 1960–2024. It assesses the extent to which trend and change-point evidence depends on temporal persistence, multiple testing and interstation consistency, and evaluates contemporaneous land-cover–discharge associations within the upstream area of each gauge. Annual MapBiomas observations for 1985–2024 were extracted within ten independently delineated contributing areas. Record-exclusion, temporal-specification and spatial-support sensitivities distinguish the consistency of the observed associations from evidence required for hydrological attribution.

2. Materials and Methods

2.1. Study Area

The Ribeira de Iguape River Basin extends across eastern Paraná and southeastern São Paulo, Brazil (Figure 1). A complementary map showing the precipitation and streamflow monitoring stations and selected hydropower facilities is provided in Figure S1 in the Supplementary Materials. The documented hydrographic vector boundary covers 25,810.3 km^2, and its intersection with the terrestrial mask covers 25,803.2 km^2 (Table S20). These measurements refine the frequently quoted approximate extent of 25,000 km^2.

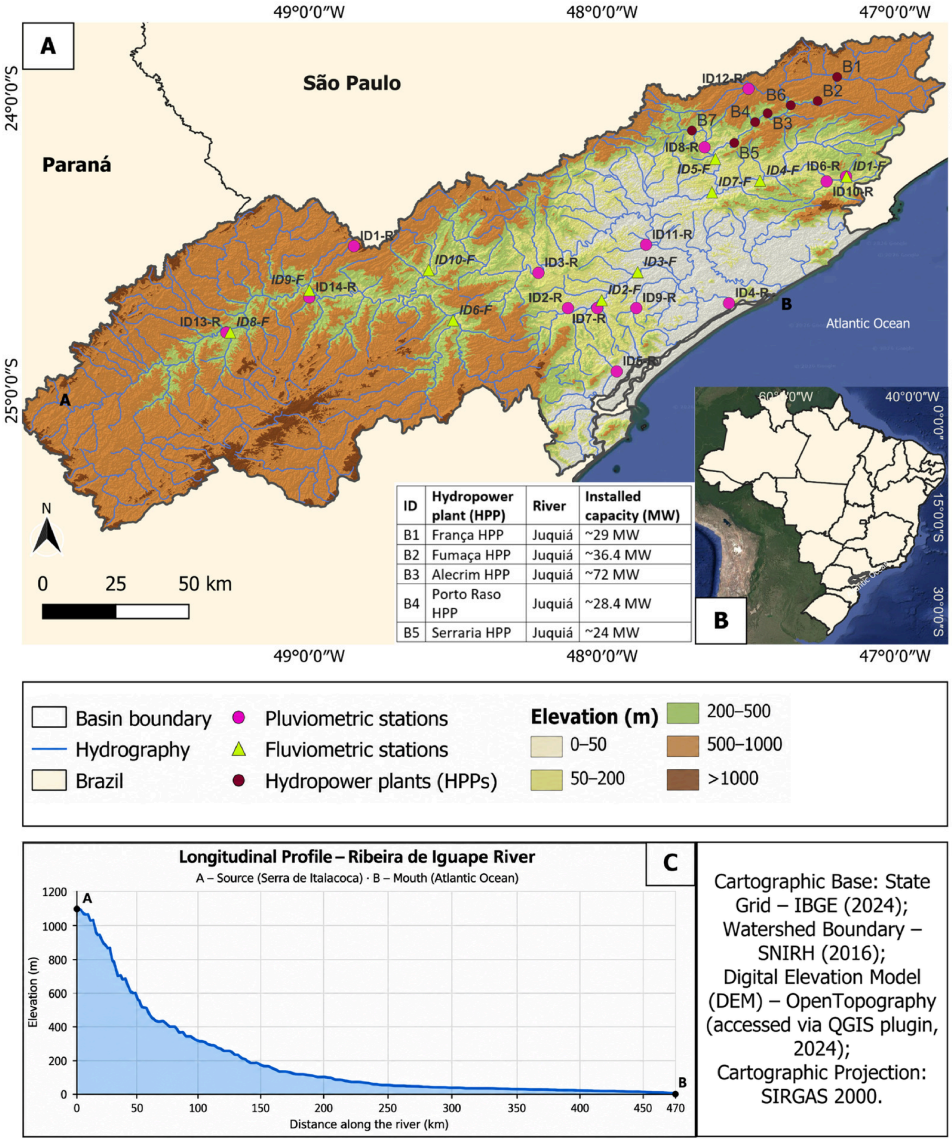


Figure 1. The Ribeira de Iguape River Basin. (**A**) Five elevation intervals (0–50, 50–200, 200–500, 500–1000 and >1000 m), hydrography, rainfall and discharge gauges, and selected Juquiá hydropower stations; (**B**) location within Brazil; (**C**) longitudinal profile of the Ribeira de Iguape River. Plant labels B1–B6 refer to the Juquiá system; B6 is Barra HPP (40.4 MW), which is not included in the inset listing of B1–B5 [24]. The source (A) and river mouth (B) labels shown within panel (**A**) indicate the endpoints of the longitudinal profile in panel (**C**); they are not additional subpanels.

The basin-scale land-cover inventory represents a distinct raster domain of approximately 26,332 km^2, about 2.0% larger than the vector boundary. Its exact boundary provenance cannot be established from the classification files. Consequently, the mapped class areas are distinguished from hydrographic basin area throughout the analysis. Class-

by-class extraction within the documented terrestrial domain is available for 1985 and 2024 (Table S23; Supplementary Data I), whereas the forty-year basin-scale trajectories retain the inventory's raster support. As a complementary analysis, exploratory associations between precipitation-network descriptors and basin-scale land-cover classes are presented in Figure S2 in the Supplementary Materials.

Approximately 62% of the regional basin lies in São Paulo and 38% in Paraná State. The São Paulo sector includes 23 municipalities and was reported to contain approximately 452,000 inhabitants [25]. The Ribeira River extends approximately 470 km from the Serra de Paranapiacaba to the Atlantic Ocean.

The basin encompasses a regional summit surface, dissected hills of the Serra do Mar, the tectonic depression of the lower Ribeira and an extensive coastal plain. This geomorphological diversity reflects the interaction of structures associated with the Brasiliano cycle, Mesozoic reactivation and subsequent climatic and coastal processes [26].

The regional climate is classified as Cfa, humid subtropical, with warm summers and no well-defined dry season. Mean annual temperature is approximately 20 °C [27], with monthly means below 18 °C in the coldest month and above 22 °C in the warmest month [28,29]. According to Galvani et al. [30], three climatic domains occur within the basin. The Subtropical domain is found in higher-elevation areas to the east, the humid mild Tropical domain occupies mainly the central and northeastern sectors, and the humid Tropical domain predominates along the coast, where temperatures and precipitation totals are higher. June, July, and August have the lowest precipitation totals, ranging from 70 to 150 mm, whereas rainfall increases between December and March, reaching 250 to 380 mm, largely due to the influence of the South Atlantic Convergence Zone (SACZ) [31].

The Cananéia–Iguape Coastal System contains coastal plains, sandy ridges and fluvial plains supporting forests and extensive mangroves [26,32,33]. Their biodiversity and productivity confer substantial ecological and socioeconomic importance [26]. Adjacent coastal sectors of Paraná also retain extensive forest, mangrove and restinga vegetation, including protected areas and vegetation in advanced stages of regeneration.

Several basin municipalities have among the lowest Human Development Index values in São Paulo State [34,35]. Infrastructure, service and economic deficiencies heighten environmental vulnerability and reinforce the need for integrated water resources planning.

2.2. Data Used

2.2.1. Streamflow Data

Annual mean (Q_{mean}), maximum (Q_{max}) and minimum (Q_{min}) streamflow were calculated from monthly series at ten stations operated by the National Water and Basic Sanitation Agency (ANA) and the São Paulo State Department of Water and Electric Energy (DAEE/SP-Águas). Q_{mean} is the arithmetic mean of the twelve monthly means, Q_{max} the largest reported monthly maximum and Q_{min} the smallest reported monthly minimum in each complete year. The source exports available for this analysis did not establish consistently whether the monthly extrema were derived from daily mean discharge or instantaneous measurements; this distinction therefore remains unverified and is not inferred from the statistical series. Table 1 gives station metadata, and Tables S1 and S2 document effective annual coverage.

Discharge records supplied by ANA and DAEE are obtained by converting stage measurements through rating curves. These relationships may change following erosion, sediment deposition, channel modification or alterations to hydraulic controls. Flood-wave hysteresis can also produce different discharges at the same stage during rising and falling limbs. Inadequately represented changes in these relationships can introduce systematic errors into the discharge series [3,36].

Table 1. Streamflow monitoring stations, official drainage areas and effective annual analysis extents within 1960–2024. Independently delineated contributing areas and their validation are reported in Table S14 and Section 3.4.

ID	Missing (%)	Code	Municipality	Watercourse	Latitude	Longitude	Official Drainage Area (km²)	Annual Extent (n)
ID1-F	2.44	4F-014	Itariri	Guanhanha River	−24.2669	−47.1653	91	1960–2022 (58)
ID2-F	6.01	81710000	Jacupiranga	Jacupiranga River	−24.6897	−48.0014	777	1960–2022 (53)
ID3-F	2.02	4F-016	Registro	Jacupiranga River	−24.5936	−47.8786	1325	1963–2024 (57)
ID4-F	0.13	81630000	Miracatu	São Lourenço River	−24.2811	−47.4606	1480	1960–2024 (64)
ID5-F	0.00	81530000	Juquiá	Juquiá River	−24.2064	−47.6133	2440	1960–2023 (64)
ID6-F	0.00	81335000	Barra do Turvo	Pardo River	−24.7586	−48.5086	2930	1977–2023 (47)
ID7-F	3.60	4F-018	Juquiá	Juquiá River	−24.3206	−47.6247	4341	1970–2024 (49)
ID8-F	0.13	81135000	Balsa do Cerro Azul	Ribeira do Iguape River	−24.8000	−49.2700	4600	1960–2023 (63)
ID9-F	0.00	81200000	Ribeira	Ribeira do Iguape River	−24.6556	−48.9997	7360	1960–2023 (64)
ID10-F	0.00	81350000	Iporanga	Ribeira do Iguape River	−24.5864	−48.5922	12,500	1960–2024 (65)

Missing (%) denotes absent months between the first and last valid observation within 1960–2024. Complete annual discharge observations require twelve months with Q_{mean}, Q_{max} and Q_{min} available simultaneously. The drainage areas in the inventory are the official source values. Independently delineated catchments were evaluated against those values without using them to select DEM outlets (Table S14; Section 3.4). Station 4F-016 lies in the municipality of Registro and is identified as Ingatuba in the DAEE inventory [37].

Interstation comparisons and relative double-mass diagnostics were used to examine departures from regional streamflow variability, particularly at Jacupiranga and Juquiá (Table S13; Figure S3). These comparisons provide an indirect assessment of consistency, but shared climatic forcing and overlapping drainage areas limit reference independence. Because rating-curve calibration histories were unavailable, agreement with regional variability cannot establish calibration stability, and station-specific departures cannot be assigned to recalibration without the corresponding hydrometric records.

2.2.2. Precipitation Data

Precipitation records were obtained from fourteen rain gauges operated by ANA and the São Paulo State Water Agency (SP-Águas). Their distribution encompasses coastal, lowland and higher-elevation sectors of the basin (Table 2; Figure 1).

Annual rainfall totals were computed only where all twelve monthly station totals were present, without substituting neighbouring observations for missing months (Table 2 and Table S1). The acquisition files do not consistently document whether ANA values were supplied as bruto or consistido, nor whether every monthly total was derived from a complete sequence of daily observations. Accordingly, the term complete year denotes compliance with the twelve-month screening rule, not independently verified daily completeness. This unresolved provenance is reported as a limitation rather than assumed to be inconsequential.

Table 2. Rain-gauge inventory, missing-month percentage and effective annual analysis extent within 1960–2024. The first and last complete years and observed n are reported for each station.

ID	Missing (%)	Code	Municipality	Rain Gauge	Elevation (m)	Latitude	Longitude	Annual Extent (n)
ID1-R	2.98	F5-019	Apiaí	Apiaí	800	−24.5050	−48.8475	1961–2023 (59)
ID2-R	2.56	F5-028	Cajati	Serrana do Sul	50	−24.7167	−48.1167	1961–2024 (58)
ID3-R	9.62	F5-013	Eldorado	Itapeuna	40	−24.5961	−48.2175	1960–2024 (54)
ID4-R	0.26	F4-028	Iguape	Iguape	3	−24.7000	−47.5667	1960–2024 (63)
ID5-R	0.26	F4-029	Cananéia	Itapitangui	7	−24.9333	−47.9500	1960–2023 (62)
ID6-R	0.90	F4-006	Itariri	Guanhanha	50	−24.2667	−47.1667	1960–2024 (61)
ID7-R	10.20	F4-017	Jacupiranga	Jacupiranga	90	−24.7167	−48.0167	1960–2016 (31)
ID8-R	0.26	F4-007	Juquiá	Capela do Porto	40	−24.1667	−47.6500	1960–2024 (64)
ID9-R	0.64	F4-016	Pariquera-Açu	Pariquera-Açu	30	−24.7167	−47.8833	1960–2024 (62)
ID10-R	1.67	F4-019	Pedro de Toledo	Pedro de Toledo	60	−24.2833	−47.2333	1960–2024 (55)
ID11-R	4.87	F4-005	Registro	Registro	20	−24.5000	−47.8500	1960–2024 (55)
ID12-R	2.05	E4-055	Tapiraí	Tapiraí	870	−23.9667	−47.5000	1960–2023 (58)
ID13-R	1.05	2449006	Cerro Azul	Balsa do Cerro Azul	270	−24.8000	−49.2831	1960–2022 (62)
ID14-R	0.13	2449000	Adrianópolis	Capela da Ribeira	180	−24.6800	−49.0000	1960–2022 (62)

Missing (%) denotes absent months within the active station period, excluding months before the first or after the last valid record. Annual values require twelve available monthly totals, with gaps permitted between complete years (Table S1). ID7-R contributes only 31 complete annual totals and has 10.2% missing months; its trend estimate is consequently interpreted cautiously, especially when compared with longer and more complete station records.

2.2.3. Land-Use and Land-Cover Data

Annual land-use and land-cover (LULC) maps for 1985–2024 were obtained from MapBiomas Collection 10 [38] and grouped as described in Table 3. Independent assessments of classification accuracy in São Paulo provide methodological context [39,40]. The local discharge analysis uses ten upstream catchments delineated from Copernicus DEM GLO90 elevations, gauge coordinates and D8 flow routing. Geometry, outlet position, upstream nesting and agreement with official drainage areas were assessed before interpretation of the local associations (Table S14; see Section 3.4). Each annual MapBiomas map was extracted at source resolution within these boundaries. Class percentages were calculated relative to the entire valid classified catchment area, rather than normalising the eight selected classes to 100%. Annual station-class areas and raster-coverage diagnostics are provided in Supplementary Data I.

MapBiomas classes were aggregated according to the methodological criteria of the Brazilian Institute of Geography and Statistics [41] and the environmental characteristics of the basin. The resulting categories permit comparison of major landscape components while retaining the class-code correspondence specified in Table 3.

Table 3. MapBiomas class aggregation for the 1985–2024 basin-scale LULC inventory. The catchment-specific discharge analysis uses eight harmonised classes extracted within independently delineated upstream areas (Tables S14, S21 and S22).

Reclassified Class	Original Classes (MapBiomas)	Description/Grouping
Forest	3 and 4	Combines Forest Formation (3) and Savanna Formation (4) within the study's Forest category. This grouping describes mapped woody cover rather than forest age or ecological condition.
Mangrove	5	The Mangrove class is maintained as a single category, given its ecological importance.
Wetland	6 and 11	Includes Floodable Forest (6) and Wetland (11), grouped as vegetation subject to seasonal or permanent inundation.
Grassland	12, 29 and 32	Predominantly herbaceous and grassy vegetation, with sparse shrubs, occurring in natural fields, rocky outcrops, and hilltops.
Agriculture/Pasture	9, 15, 20, 21, 35, 39, 40, 41, 46, 47, 48 and 62	Combination of the classes Pasture, Agriculture (temporary and perennial), Forestry, and Mosaic of agricultural uses.
Beach	23	Covers areas of beach, dunes, and coastal or river sandbanks without significant vegetation cover.
Urban area	24	Areas occupied by urban infrastructure, buildings, and roads.
Mining	30	Areas used for mineral extraction, with clear exposure of the soil due to human activity.
Restinga Forest	49	Tree formations typical of coastal areas on sandy soils or dunes.
Restinga Herbaceous	50	Herbaceous formations established on sandy soils or coastal dunes.
Other non-vegetated	25 and 75	Areas without significant vegetation cover, including exposed soil, impervious surfaces, or landslides.
Rivers, Lakes & Ocean	31 and 33	Records of rivers, lakes, reservoirs, dams, oceans, and aquaculture are maintained.

Combined geospatial and hydrological assessment has also been applied in the Jacaré-Guaçu Basin, São Paulo [42]. The twelve-class basin-scale inventory and the eight-class catchment analysis have different spatial supports. The former describes landscape trajectories over the mapped raster domain, whereas the latter pairs annual land-cover percentages with discharge observations from the same year and upstream area. Associations obtained from alternative station polygons are reported separately as a spatial-support comparison (Tables S5, S6 and S11–S11c; Figure S5); those polygons do not define the principal hydrological units. Catchment-area validation is presented in Table S14 and Section 3.4. The Q_{mean}, Q_{min} and Q_{max} association matrices are presented with the catchment-specific results in Section 3.4. Table S21 summarises the testing families, Table S22 examines the ID3-F water class, and Supplementary Data I contains all 240 planned primary comparisons, including twelve non-estimable combinations, with sample sizes, coefficients, nominal probabilities and metric-specific and pooled BH-adjusted probabilities.

2.3. Data Preprocessing and Consistency

Hydroclimatic analyses use available observations within each station's active period. Monthly missingness is assessed between the first and last available record, and annual indices require twelve available monthly values. Missing months and annual records are not interpolated, extrapolated or replaced from neighbouring stations. For precipitation, a complete set of supplied monthly totals does not itself establish that every underlying day was observed; the original daily aggregation and bruto/consistido metadata were not fully documented in the available exports (Tables S1 and S13b).

Infilling discharge records can introduce substantial uncertainty because precipitation–stage–discharge relationships are nonlinear, seasonally variable and sensitive to extreme events [43–45]. Incomplete years were therefore excluded, even where this reduced the annual sample size.

The ID1-F observations for 2020 and 2022 were examined because annual runoff depth, calculated using the official drainage area, exceeded regional-network precipitation by factors of 4.26 and 5.52, respectively (Table S17b). These ratios compare different spatial supports and therefore serve as plausibility diagnostics, not physical runoff coefficients or proof of measurement error. The principal figures use the full source record. A separate sensitivity analysis excludes both years for Q_{mean}, Q_{max} and Q_{min}. The isolated 2024 Q_{min} value at ID7-F is examined through a one-year exclusion. Full-record and exclusion results are reported separately, without classifying an observation as erroneous solely because of its magnitude or influence (Table S17c,d).

Station-level hydroclimatic analyses retain complete observed years and their intervening gaps within 1960–2024. Catchment-specific land-cover percentages cover 1985–2024, and each discharge association uses only valid annual land-cover–discharge pairs, without interpolation. Full-record estimates constitute the principal scenario; the specified ID1-F and ID7-F exclusions are sensitivity cases. Network-weighting comparisons use identical stations and common observation years within each variable (Tables S12, S17c,d, S18, S21 and S22).

2.4. Statistical Methods

2.4.1. Trend Analysis

Annual trends were assessed with the Hamed–Rao modified Mann–Kendall test (HR-MK), which adjusts the variance of the rank statistic for serial autocorrelation [46,47] and addresses its influence on trend significance in hydroclimatic records [47,48]. The test was applied separately to precipitation, Q_{mean}, Q_{max} and Q_{min}. Kendall's τ describes the direction and strength of monotonic ordering [49], while Sen's median pairwise slope estimates trend magnitude [50], expressed in mm decade^{-1} for precipitation and m^3 s^{-1} decade^{-1} for discharge.

Benjamini–Hochberg adjustment [51] was applied within each annual variable family, comprising fourteen precipitation stations or ten discharge stations. Adjusted probabilities are denoted q; $q \leq 0.05$ was treated as evidence robust to the specified false-discovery adjustment, whereas $p \leq 0.05$ with $q > 0.05$ was retained as nominal evidence. In the spatial syntheses, filled triangles denote $q \leq 0.05$, open triangles denote nominal evidence, and grey circles denote $p > 0.05$; categories absent from a figure are omitted from its legend. Calendar lag-1 autocorrelations were calculated before and after linear detrending using pairs of observations exactly one year apart. Complementary linear trend tests used Bartlett-kernel heteroskedasticity- and autocorrelation-consistent (HAC) covariance estimates at fixed lags of 1, 3 and 5 years [52]. Conditional 95% Sen intervals were obtained from 1999 residual moving-block replicates over the longest uninterrupted run of at least twenty years [53] (Tables S7 and S8); these pointwise intervals and linear tests differ from the full-record HR-MK analysis in temporal support, trend formulation, or both.

2.4.2. Change-Point Detection

Candidate level changes in annual precipitation and discharge were evaluated with Pettitt, the Standard Normal Homogeneity Test (SNHT) and the Buishand Range test. Pettitt maximises an absolute rank-based statistic comparing two segments without requiring a particular continuous distribution [54], whereas SNHT uses a variance-standardised statistic for a change in the mean [55] and Buishand evaluates the range of cumulative deviations from the series mean [56]. Applying the three criteria to the same observations permits assessment of both candidate timing and its sensitivity to the form of the change statistic.

The tests were applied in parallel to compare candidate timing [57–59], recognising that their classical probability formulations assume serial independence. The observed

maximum statistics were therefore also evaluated under null models retaining temporal dependence. Estimated dates identify statistical splits within the available record, while evidence of climatic, hydrometric or operational intervention requires information beyond agreement among test dates.

Benjamini–Hochberg (BH) adjustment was applied separately by variable and by change-point test. Classical Pettitt, SNHT and Buishand results were compared with moving-block permutations on uninterrupted records and 9999 full-record Gaussian first-order autoregressive [AR(1)] simulations preserving the actual calendar gaps (Table S10b,c). The AR(1) parameter φ was estimated by exact Gaussian profile likelihood under three specifications: the original series, linearly detrended residuals, and residuals demeaned separately before and after the test-specific candidate year. The latter specification is conditional on the estimated split and therefore cannot independently confirm it. For ID14-R precipitation, the raw φ estimate of 0.650 falls to 0.531 after detrending and to 0.473–0.497 after segment demeaning (Table S10d). These alternatives assess the sensitivity of nominal change-point evidence to persistence estimation; they are not equivalent independent tests. Dates with fewer than eight observed years on either side are described as poorly supported statistical candidates, not as established transitions.

Seasonal analyses used DJF, MAM, JJA and SON, requiring observations for all three constituent months. DJF was assigned to its January–February year. Precipitation totals were summed, Q_{mean} values averaged, and monthly extrema used to determine seasonal Q_{max} and Q_{min}. Sen estimates and HAC sensitivities were calculated for 176 station–variable–season combinations. BH families included all four seasons within each variable (Table S9). These meteorological seasons are distinct from the calendar quarters used for climatological description in Figure 2.

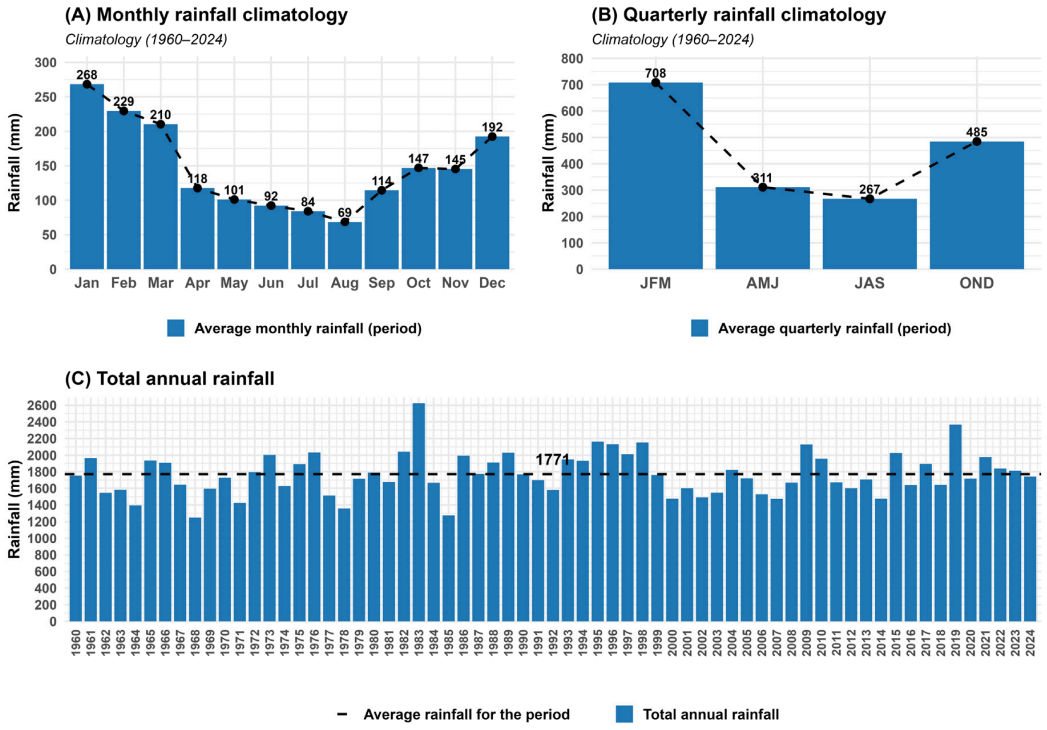


Figure 2. Precipitation variability within the 1960–2024 regional analysis window. (**A**) Monthly climatology; (**B**) calendar-quarter totals for JFM, AMJ, JAS and OND; (**C**) annual network precipitation. Station coverage varies as documented in Table 2 and Table S1. The seasonal trend supplement uses DJF, MAM, JJA and SON.

2.4.3. Catchment-Specific LULC–Discharge Associations and Spatial Support

Catchment-specific land-cover–discharge associations were estimated from 40 annual MapBiomas Collection 10 maps within ten DEM-delineated upstream areas. For each of Q_{mean}, Q_{min} and Q_{max}, annual discharge was paired with the percentage of eight harmonised classes using complete observed year-pairs within 1985–2024. The design comprises 240 comparisons, of which twelve are non-estimable because the corresponding class is absent or constant. The resulting testing families contain 76 estimable coefficients per discharge metric and 228 coefficients overall (Table S21). Non-estimable cells remain explicitly identified in Supplementary Data I and are not represented as zero correlations. The 75-test families reported in the spatial-support comparison refer to alternative station polygons, not to these DEM-delineated catchments (Tables S5, S6 and S11a–c).

Contributing areas were derived from Copernicus DEM GLO90, gauge coordinates and D8 flow accumulation. Outlet selection used proximity to the gauge and the DEM-derived drainage network; official drainage-area values were reserved for subsequent validation rather than used to force area agreement. All ten delineations met the prespecified ±10% area-difference criterion and the upstream-topology checks. Differences from official area were +1.2% at ID1-F, +1.0% at ID3-F and −9.4% at ID6-F (Table S14; Section 3.4). Across 480 domain–year coverage checks, the largest absolute raster–vector area discrepancy was 0.016%. These diagnostics evaluate geometrical consistency and extraction completeness; they do not validate rating curves, source station identifiers, individual land-cover classifications or causal hydrological relationships. ID6-F remains close to the area-screening threshold.

As a separate exploratory exercise, twelve basin-wide land-cover classes were compared with regional precipitation-network descriptors, yielding 108 temporally paired comparisons. These descriptors have a different spatial support from station-specific discharge and cannot be interpreted as precipitation responses to land-cover change (Supplementary Figure S2; Tables S5 and S6). The principal local analysis instead relates discharge to land-cover percentages within each independently delineated upstream catchment (Section 3.4). Network-weighting sensitivities use common observation years and compare equal, drainage-area and mean-discharge weights without treating partly nested basins as independent sampling units (Tables S12 and S18).

The principal local analysis uses contemporaneous Pearson correlations. Benjamini–Hochberg (BH)-adjusted probabilities were calculated separately for the complete set of 76 estimable comparisons for each discharge metric and for the pooled family of 228 comparisons. Unadjusted p values and the two corresponding q values are reported separately in Supplementary Data I, whereas Table S21 summarises their inferential classifications. Spearman coefficients, detrended relationships, first differences between consecutive years, alternative windows and denominators, and the hydrometric exclusion scenarios were analysed as complementary specifications (Tables S21 and S22; Supplementary Data I). The BH procedure controls the declared multiple-testing family but does not correct serial dependence in the original Pearson tests, dependence among nested catchments or omitted hydroclimatic drivers. Sensitivity outcomes are therefore not treated as independent confirmation of contemporaneous associations or as causal estimates.

Relative consistency was investigated by comparing each selected discharge station with a leave-one-out regional reference, using station/reference ratios and double-mass curves (Table S13; Figure S3). The same approach was extended to rainfall at Guanhanha (ID6-R), Balsa do Cerro Azul (ID13-R) and Capela da Ribeira (ID14-R). Reference values were drawn from concurrently available gauges and normalised before comparison (Table S13b). Persistent relative departures are evidence of differences among records,

but cannot distinguish a local climatic anomaly from a change in instrumentation, site conditions or data processing without station metadata.

Basin LULC trends for 1985–2024 were assessed using HR-MK and Sen's slope. The twelve reclassified classes constituted the BH trend family, and slopes are expressed in km^2 $decade^{-1}$. An independent assessment of rank ordering and successive annual changes is provided in Table S15.

Pettitt, SNHT and Buishand Range tests were also applied to the annual basin class areas. Probabilities were adjusted across the twelve classes separately for each test, using $q \leq 0.05$ as the significance criterion. These classical candidates describe contrasts within evolving area trajectories and are not independently verified dates of land conversion. Complete results were retained for all classes. The five classes with the lowest HR-MK q values among those meeting the trend criterion were selected for graphical presentation.

2.5. Hydrological Context for Spatial Interpretation

The hydrology of the Ribeira de Iguape River Basin is strongly influenced by the region's humid climate and the contrast between plateau and lowland areas. Streamflow reflects the seasonality of precipitation, with higher values during summer and lower values during winter, although no well-defined dry season occurs. The official characterisation of regional water resources also emphasises internal contrasts within the basin and the need to consider relief, drainage, water availability, and water use jointly in regional planning [60].

The altitudinal gradient imposed by the Serra do Mar influences the hydrological response of tributaries. In mountainous areas, steep slopes favour rapid responses to rainfall events. In lower-gradient reaches, particularly in the middle and lower Ribeira sectors, streamflow responses are more attenuated.

Vegetation influences infiltration, evapotranspiration and baseflow, while intensive land use can modify runoff pathways. These processes provide a physical framework for interpretation but were not directly quantified. Annual runoff depths were screened against regional network precipitation using official drainage areas (Table S17a,b). Catchment-integrated precipitation and potential evapotranspiration were unavailable, precluding estimation of physical runoff coefficients or Budyko elasticities.

The Jacupiranga, Juquiá, Pardo, and São Lourenço subbasins exhibit distinct drainage and land-use patterns, resulting in different hydrological responses. Individual analysis of streamflow series was therefore maintained to preserve these spatial differences in the subsequent statistical analyses.

3. Results

The results distinguish annual trends, candidate level changes and catchment-specific land-cover–discharge associations. Temporal-dependence, interstation and record-exclusion diagnostics are used to identify findings whose interpretation changes across analytical specifications. These analyses describe different properties of the observations and are not treated as independent confirmation of a common hydroclimatic mechanism.

3.1. Precipitation

3.1.1. Temporal Characterisation

Regional precipitation exhibits pronounced seasonality and interannual variability within the 1960–2024 analysis window. Station-specific complete-year coverage is reported in Table 2. Mean annual network precipitation is approximately 1771 mm, with totals exceeding 2500 mm in 1983 and remaining below 1300 mm in 1968 and 1985. These values characterise the observed gauge network rather than catchment-integrated precipitation.

Approximately 40% of annual precipitation occurs during JFM, which receives about 708 mm (Figure 2B). This concentration is consistent with the influence of the SACZ, cold fronts and summer convection in southeastern Brazil [31]. Totals decline to approximately 311 mm in AMJ and 267 mm in JAS. August has the lowest monthly mean, approximately 69 mm (Figure 2A). Cold fronts and maritime influence sustain rainfall during the less rainy months, while the OND total of approximately 485 mm marks the return to wetter conditions.

Interannual precipitation alternates between markedly wetter and drier years (Figure 2C). Regional atmospheric systems and large-scale teleconnections, particularly the El Niño–Southern Oscillation (ENSO), contribute to rainfall variability in southeastern Brazil [61,62]. Their influence varies spatially and between ENSO phases, as documented for southeastern South America and other Brazilian basins [63–66]. The present analysis does not quantify individual teleconnection contributions.

3.1.2. Trends and Change Points

Eight of the fourteen gauges showed annual precipitation trends remaining significant after BH adjustment: seven positive and one negative (Serrana do Sul, ID2-R). The largest positive Sen slopes occurred at Balsa do Cerro Azul (+101.5 mm decade^{-1}), Guanhanha (+98.3 mm decade^{-1}) and Capela da Ribeira (+90.1 mm decade^{-1}). These values describe the original station series; the relative-consistency evidence for the first and third stations does not justify treating their unusually large increases as unequivocal climatic change (Tables S2, S10d and S13b).

Balsa do Cerro Azul (ID13-R) has a positive annual Sen slope of +101.5 mm decade^{-1} (HR-MK $q < 0.001$), with 1981 selected by all three classical change-point tests (Figure 3A). The post-1981 segment mean exceeds the earlier mean by 47.7%, but the station/reference median and relative double-mass slope also increase by 41.4% and 40.8%, respectively (Table S13b). These sizeable departures indicate that the station does not follow the same proportional evolution as the reference gauges. They do not, however, establish whether the source is local climate variability, observational inhomogeneity or both. Dependence-based tests retain different levels of support according to the AR(1) specification (Table S10d).

Capela da Ribeira (ID14-R) shows a positive annual Sen slope of +90.1 mm decade^{-1} (HR-MK $q = 0.006$; Figure 3B). Pettitt and Buishand identify 1981, while SNHT selects 1972. Across the 1981 split, the segment mean increases by 52.7%, alongside changes of 34.2% in the relative station/reference median and 44.0% in the double-mass slope (Table S13b). A raw annual AR(1) parameter of 0.650 is reduced by detrending or segment demeaning, with correspondingly variable adjusted change-point probabilities (Table S10d). The disagreement in candidate dates and relative record variability limits interpretation of the apparent step as a regional climate signal.

At Apiaí (ID1-R) and Itapeuna (ID3-R), positive annual Sen slopes are +48.2 and +38.2 mm decade^{-1}, respectively, both surviving BH adjustment (Figure 3C,D). Their classical change-point candidates do not retain adjusted support; the evidence therefore concerns gradual monotonic tendency rather than an identified abrupt transition.

Serrana do Sul (ID2-R) is the only gauge with an FDR-robust decreasing annual precipitation trend (Sen −34.3 mm decade^{-1}; $q = 0.006$; Figure 4A). No classical change-point test meets the adjusted criterion.

Pariquera-Açu (ID9-R) and Tapiraí (ID12-R) show positive Sen slopes of +28.5 and +26.2 mm decade^{-1}, respectively (HR-MK $q = 0.031$ and 0.026; Figure 4B,C). The corresponding classical candidate changes are not supported after BH adjustment.

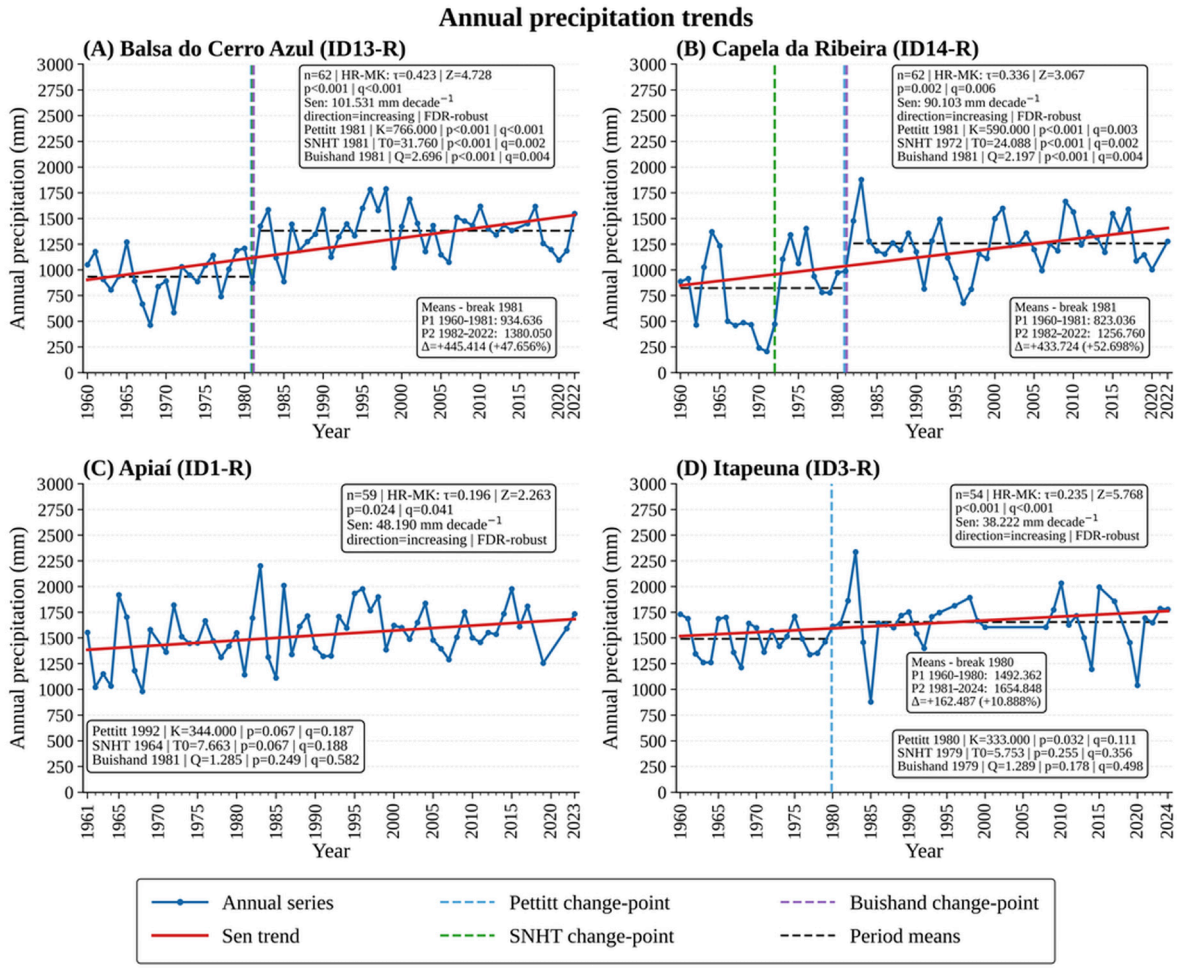


Figure 3. Annual precipitation trends and change points. (**A**) Balsa do Cerro Azul (ID13-R); (**B**) Capela da Ribeira (ID14-R); (**C**) Apiaí (ID1-R); (**D**) Itapeuna (ID3-R). Panels show HR-MK results, Sen's slope, and change points evaluated using the Pettitt, SNHT, and Buishand tests.

Guanhanha (ID6-R) has a positive annual precipitation Sen slope of +98.3 mm decade^{-1} (BH $q < 0.001$; Figure 4D). Pettitt and Buishand select 1980 without adjusted support, whereas SNHT identifies 2018 with only five valid annual observations thereafter. A separate 1981-based comparison indicates a 23.3% increase in station mean precipitation, against 10.9% in the median station/reference ratio and 15.2% in the double-mass slope (Table S13b). The candidate timing, unequal reference trajectories and limited post-2018 support do not resolve whether the change is climatic or related to the observational series.

Figure 5 summarises the annual rainfall evidence without converting statistical candidate dates into verified regime shifts. Seven gauges have BH-supported increasing trends, Serrana do Sul has a BH-supported decrease, and classical change-point support is concentrated at a few stations. The large 1981 shifts at Balsa do Cerro Azul and Capela da Ribeira coincide with relative interstation departures; at Guanhanha, the SNHT-supported 2018 candidate rests on only five subsequent observations. These qualifications are central to interpretation of the spatial pattern, although they do not alter the station-level HR-MK symbols (Tables S3, S10a–d and S13b).

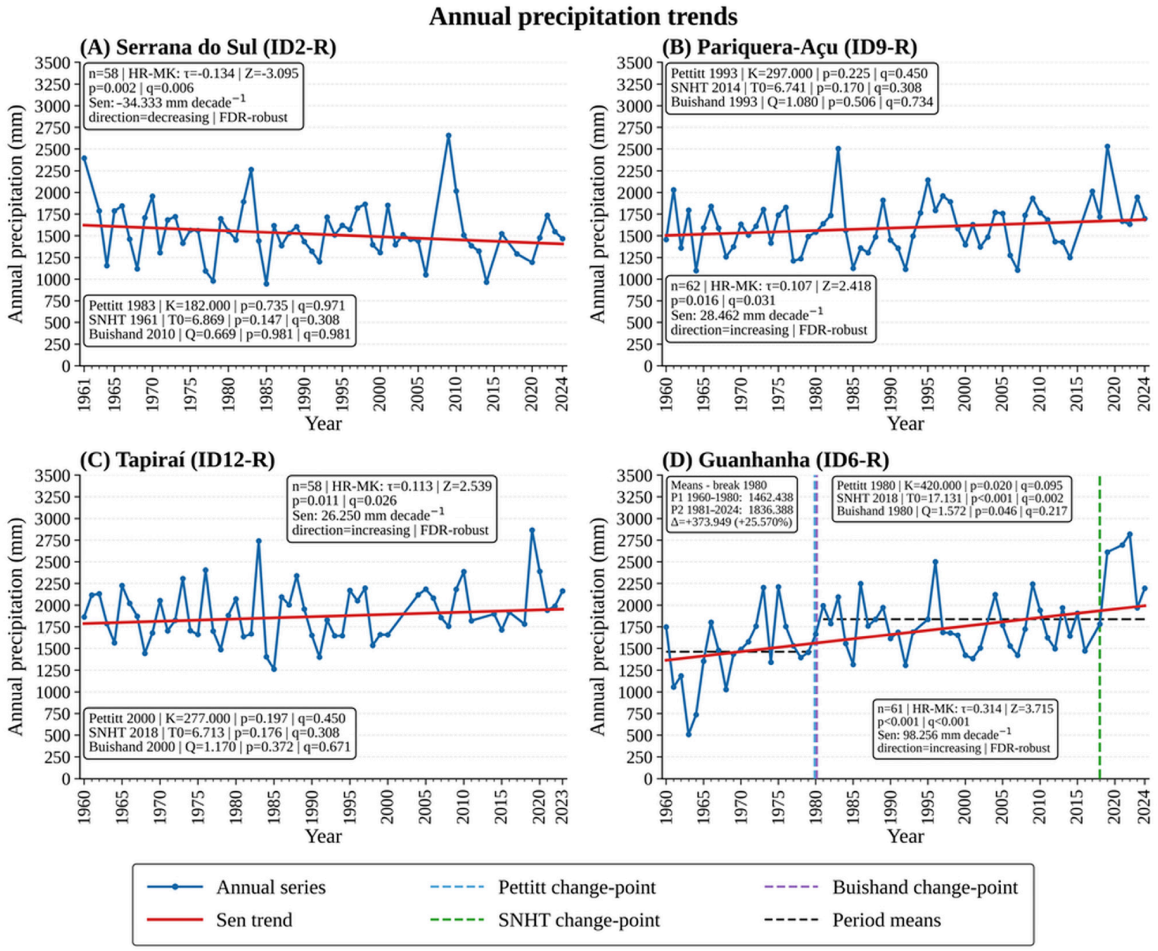


Figure 4. Annual precipitation trends and change points. (**A**) Serrana do Sul (ID2-R); (**B**) Pariquera-Açu (ID9-R); (**C**) Tapiraí (ID12-R); (**D**) Guanhanha (ID6-R). Panels show HR-MK results, Sen's slope, and change points evaluated using the Pettitt, SNHT, and Buishand tests.

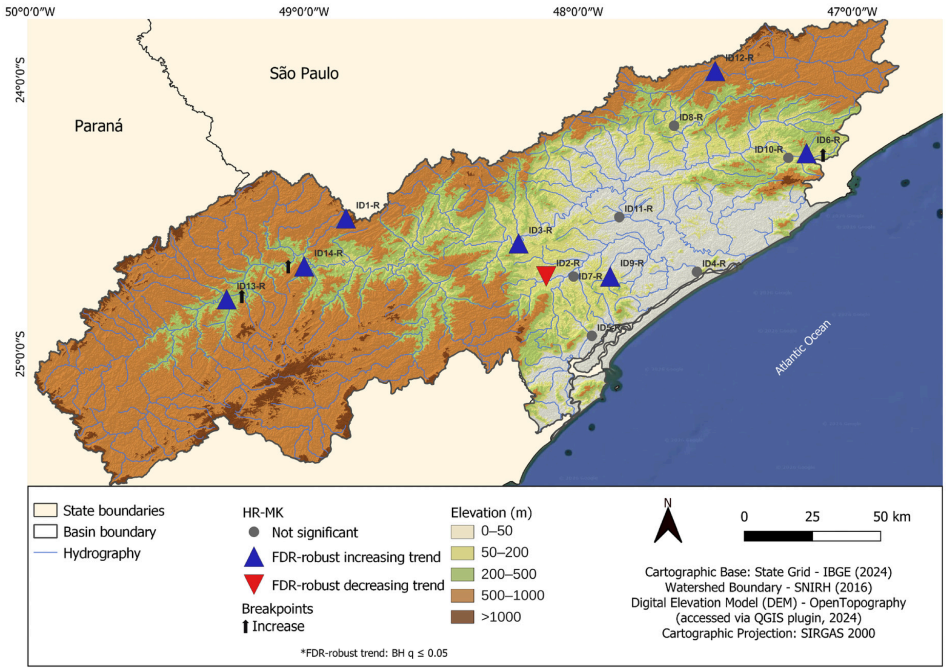


Figure 5. Spatial synthesis of annual precipitation HR-MK trends and classical change-point evidence. Blue and red filled triangles indicate increasing and decreasing trends that remain significant after

BH adjustment ($q \leq 0.05$), and grey circles denote $p > 0.05$. Black arrows identify stations where at least one classical change-point test retains $q \leq 0.05$ within its BH family; arrow direction follows the post- minus pre-candidate segment-mean contrast. At Guanhanha, the mapped arrow is based on SNHT alone and the 2018 split has short post-candidate support (Table S10). Dependence sensitivities are reported in Tables S7 and S10c.

3.2. Streamflow Trends and Change Points

Streamflow patterns are less spatially coherent than precipitation and differ among Q_{mean}, Q_{max} and Q_{min}. The following figures present the annual HR-MK and classical change-point results, while Tables S7–S13 provide dependence, segment-support and interstation diagnostics that indicate whether the same directional or level-change signal persists under complementary formulations.

Juquiá (ID5-F) is the only streamflow station with an annual HR-MK trend that survives BH adjustment: Q_{max} decreases by -16.2 m^3 s^{-1} decade^{-1} ($q < 0.001$; Figure 6C). Its consecutive-record moving-block interval supports a negative slope, while the alternative HAC linear-trend specification does not retain BH-adjusted significance (Tables S7 and S8). At Jacupiranga (ID2-F), Q_{mean} and Q_{min} increase nominally by +1.3 and +0.3 m^3 s^{-1} decade^{-1}, and Balsa do Cerro Azul (ID8-F) shows a nominal Q_{max} increase of +51.7 m^3 s^{-1} decade^{-1}. None of these three positive results survives the original HR-MK BH adjustment.

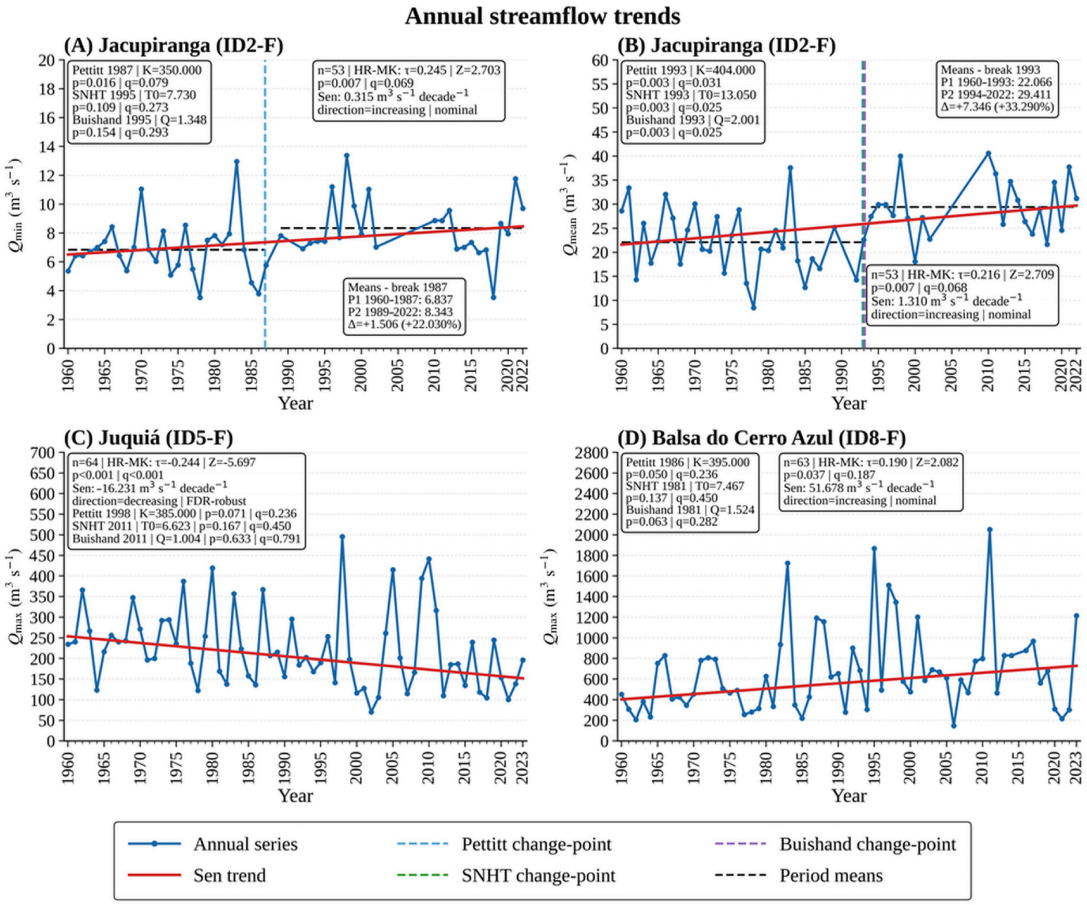


Figure 6. Annual streamflow estimates and candidate change points. (**A**) Jacupiranga Q_{min}; (**B**) Jacupiranga Q_{mean}; (**C**) Juquiá Q_{max}; (**D**) Balsa do Cerro Azul Q_{max}. Displayed HR-MK and classical change-test probabilities use within-variable BH families. Complementary evidence is reported separately in Tables S7, S8 and S10c. At Jacupiranga (panel (**B**)), Pettitt, SNHT and Buishand all identify 1993; their dashed indicators coincide, so the green SNHT line is not separately visible.

At Jacupiranga (ID2-F), all three classical tests identify 1993 as the Q_{mean} candidate, with segment means of 22.1 and 29.4 $m^3\ s^{-1}$ (+33.3%). This result meets the classical BH criterion but is less robust to full-record AR(1) sensitivity, and the longest uninterrupted subrecord ends before the candidate date. Its timing is consequently described as a statistical contrast rather than a confirmed intervention or regime transition (Table S10a–d).

At Balsa do Cerro Azul (ID8-F), Q_{min} means are 39.5 and 47.8 $m^3\ s^{-1}$ on either side of the 1994 candidate (+20.9%; Figure 7A). Buishand alone survives BH adjustment (q = 0.043), limiting agreement among tests.

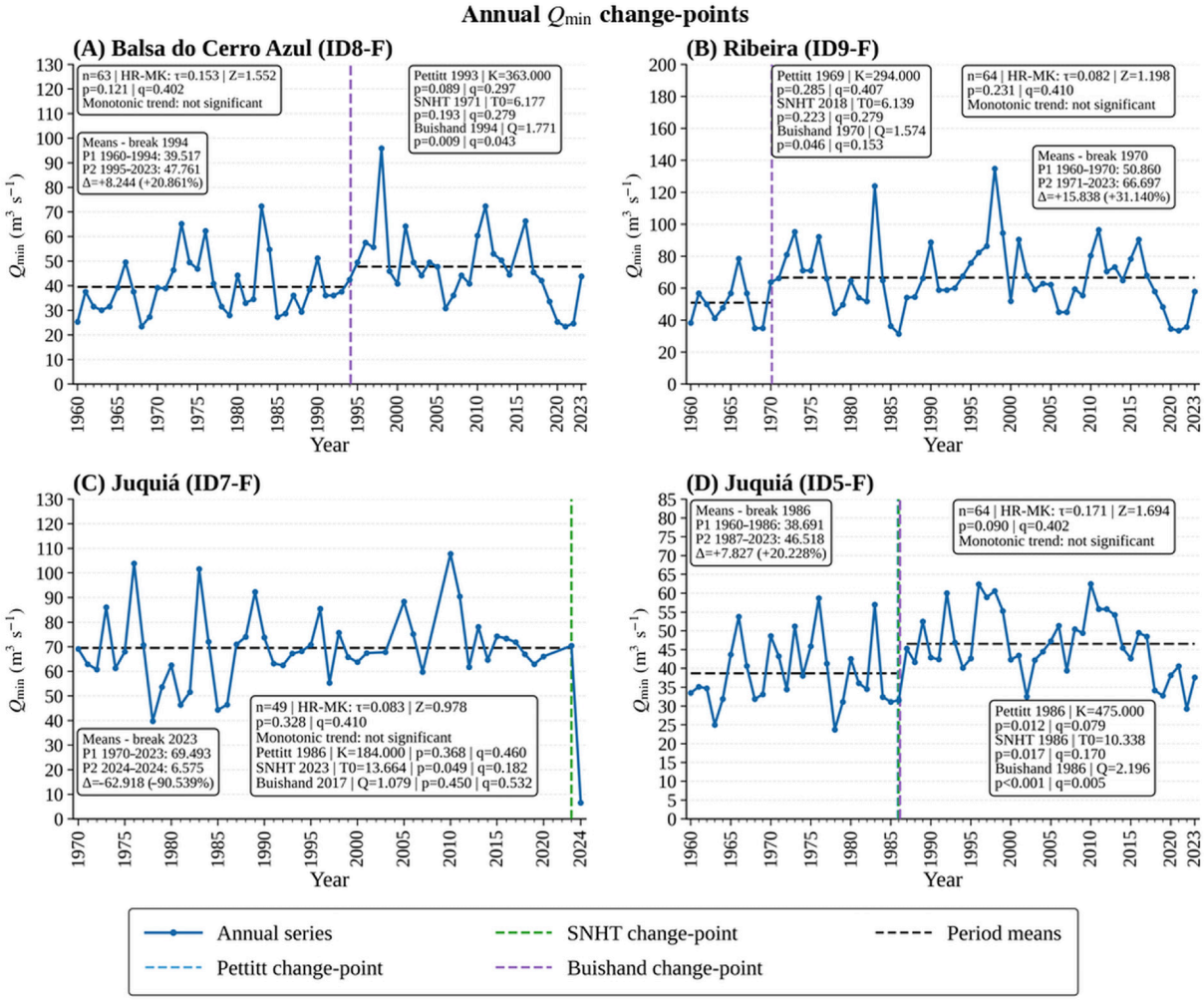


Figure 7. Change points in annual minimum streamflow. (**A**) Balsa do Cerro Azul (ID8-F); (**B**) Ribeira (ID9-F); (**C**) Juquiá (ID7-F); (**D**) Juquiá (ID5-F). Panels show segment means and results from the Pettitt, SNHT, and Buishand tests.

At Ribeira (ID9-F), classical tests identify Q_{min} candidates between 1969 and 2018, with none significant after BH adjustment (Figure 7B). Differences between the plotted segment means are consequently descriptive and do not establish a sustained change in the discharge regime.

At downstream Juquiá (ID7-F), no annual Q_{min} trend or classical change-point candidate survives BH adjustment (Figure 7C). The SNHT candidate in 2023 is based on a single subsequent annual observation, $Q_{min} \approx 6.6\ m^3\ s^{-1}$ in 2024. Such a short segment cannot establish a change in regime. Removing the 2024 observation increases the annual Sen slope from +0.9 to +1.3 $m^3\ s^{-1}$ $decade^{-1}$ but does not produce a BH-supported trend;

the candidate dates and adjusted support also change under the exclusion (Table S17c,d). This isolated value remains subject to source-record verification.

At Juquiá (ID5-F), Q_{min} means increase from 38.7 to 46.5 m^3 s^{-1} across the 1986 candidate (+20.2%; Figure 7D). Buishand alone survives BH adjustment (q = 0.005); the other classical tests do not.

At Balsa do Cerro Azul (ID8-F), mean discharge before and after the 1992 candidate is 76.3 and 93.0 m^3 s^{-1}, respectively (Figure 8A). Neither the HR-MK trend nor the candidate change-point tests survive multiplicity adjustment.

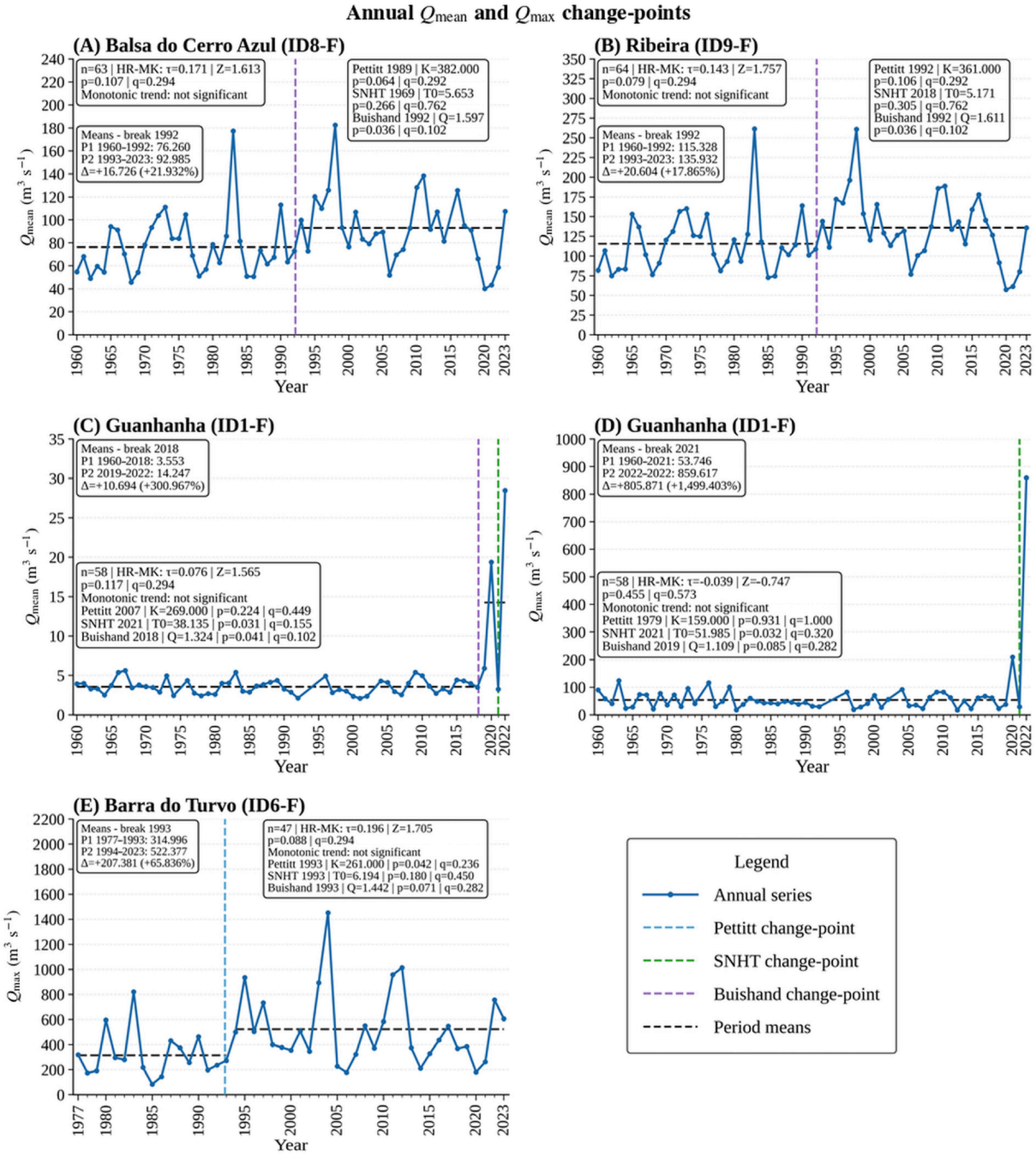


Figure 8. Annual mean-discharge contrasts at (**A**) ID8-F, (**B**) ID9-F and (**C**) ID1-F, and maximum-discharge contrasts at (**D**) ID1-F and (**E**) ID6-F. The ID1-F contrasts in panels (**C**,**D**) have only four and one subsequent observations; see Table S17c,d for record-exclusion sensitivities.

At Ribeira (ID9-F), Q_{mean} means are 115.3 and 135.9 $m^3\ s^{-1}$ across the 1992 candidate (Figure 8B). The contrast is descriptive because neither the trend nor the classical change-point evidence retains BH support.

At Guanhanha (ID1-F), the original Q_{mean} split in 2018 has only four later observations, while the Q_{max} candidate in 2021 has only one. The resulting approximate segment-mean differences of +301% and +1499%, respectively, are therefore highly sensitive descriptive contrasts, not reliable estimates of persistent changes (Figure 8C,D). The exclusion of the questioned 2020 and 2022 observations changes the Q_{max} Sen slope from -0.9 to -2.3 $m^3\ s^{-1}$ $decade^{-1}$, yielding nominal evidence (HR-MK $p = 0.043$) but not significance in the complete BH-adjusted ten-station family (q = 0.143). The screened Q_{mean}, Q_{min} and Q_{max} change-point results likewise do not demonstrate an abrupt transition (Table S17b–d).

At Barra do Turvo (ID6-F), Q_{max} means are 315.0 and 522.4 $m^3\ s^{-1}$ across the 1993 candidate (+65.8%; Figure 8E). Neither the original trend nor any classical candidate survives BH correction, so the difference is not evidence of a confirmed abrupt shift.

Figure 9 retains one FDR-robust annual streamflow trend, the decreasing Q_{max} at Juquiá (ID5-F). The positive Q_{mean} and Q_{min} trends at Jacupiranga and Q_{max} at Balsa do Cerro Azul remain nominal. Classical change-point arrows summarise the 1993 Jacupiranga Q_{mean} candidate, supported by all three tests, and two Q_{min} contrasts supported by Buishand alone. None of the original Q_{max} change-point candidates survives BH adjustment. The record-exclusion scenarios for ID1-F and ID7-F do not alter the classification of BH-supported annual streamflow trends shown in Figure 9. Seasonal sensitivities and full-family adjustment are documented in Tables S9, S12 and S17c.

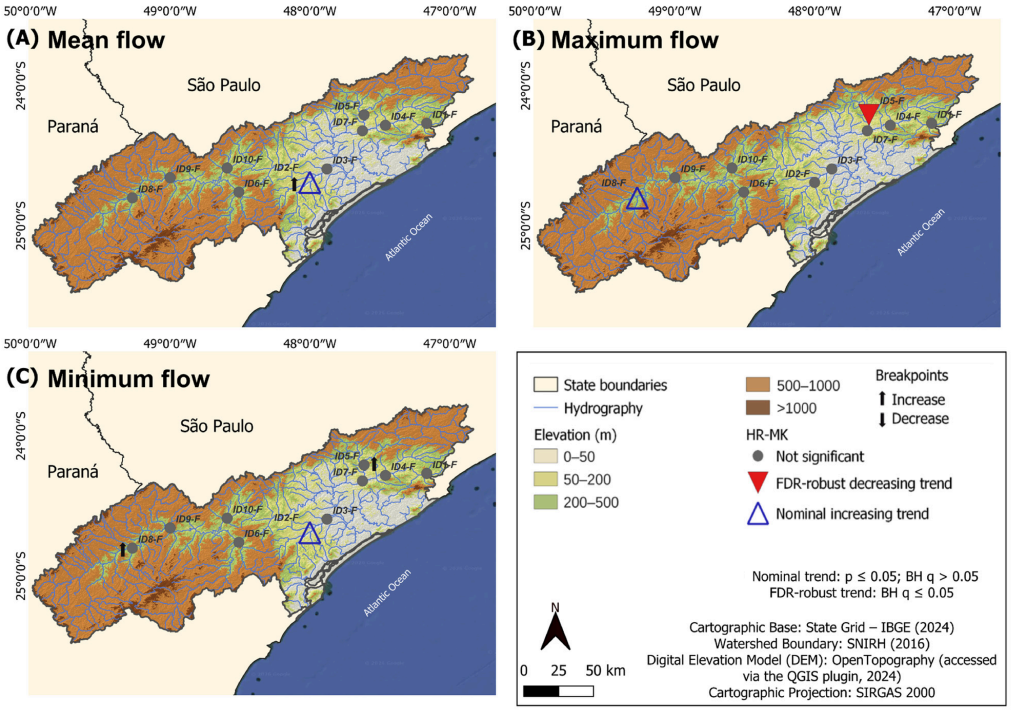


Figure 9. Spatial synthesis of annual streamflow HR-MK trends and classical change-point evidence for (**A**) Q_{mean}, (**B**) Q_{max} and (**C**) Q_{min}. The filled red triangle denotes the FDR-robust decreasing trend (BH q $\leq$ 0.05), open blue triangles denote nominal increasing evidence ($p \leq 0.05$; BH q > 0.05), and grey circles denote $p > 0.05$. Black arrows mark classical change-point evidence retaining q $\leq$ 0.05 after within-variable BH adjustment, with direction based on the segment-mean contrast. Dependence and segment-support sensitivities are reported in Tables S7 and S10a–c.

3.3. Land-Use and Land-Cover Changes and Trends

Forest remained the dominant basin LULC class throughout 1985–2024. Other classes exhibited contrasting changes in area and relative extent (Figure 10; Table 4). Maps for 1985, 1993, 2015 and 2024 provide a spatial representation of these trajectories.

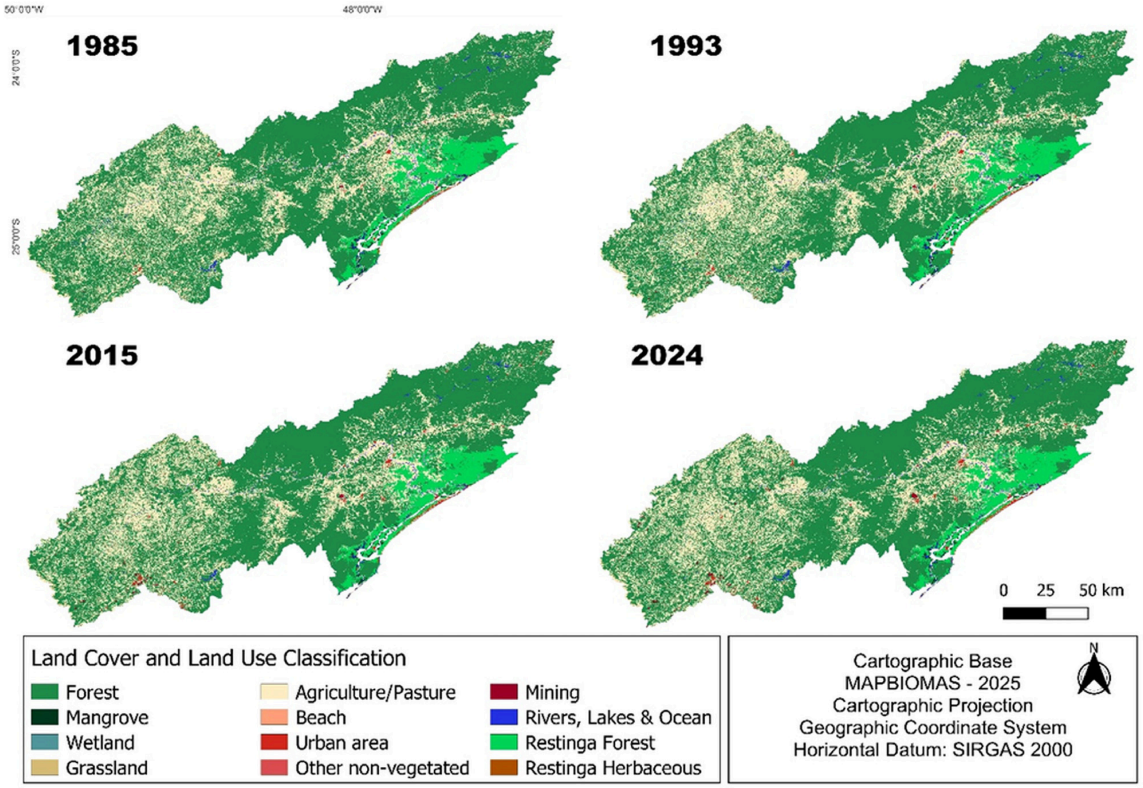


Figure 10. Land use and land cover in the Ribeira de Iguape River Basin in 1985, 1993, 2015, and 2024.

Table 4. Areas and relative changes in twelve MapBiomas land-cover classes between 1985 and 2024 on the basin-scale raster domain (approximately 26,332 km^2). This domain also underlies Figures 10 and 11. The documented terrestrial basin covers 25,803.2 km^2; its independently extracted endpoint areas are reported in Table S23, with domain differences in Table S20.

Class	1985 (km^2)	1993 (km^2)	2015 (km^2)	2024 (km^2)	Change (%)
Forest	17,166.5	16,755.3	17,015.4	17,053.2	−0.7
Mangrove	90.6	88.6	85.2	79.8	−11.9
Wetland	108.2	106.4	120.3	113.9	5.3
Grassland	61.9	64.2	75.5	61.5	−0.5
Agriculture/Pasture	6914.0	7323.1	7026.5	6956.0	0.6
Beach	7.5	6.0	4.4	5.1	−31.8
Urban area	48.3	61.9	108.1	128.7	166.3
Other non-vegetated	31.1	13.7	15.8	17.2	−44.6
Mining	9.6	16.9	33.7	49.5	415.5
Rivers, Lakes & Ocean	198.9	217.3	163.8	167.7	−15.7
Restinga Forest	1662.0	1644.5	1652.2	1669.1	0.4
Restinga Herbaceous	33.7	34.4	31.4	30.3	−10.0

Note: The historical classified raster totals 26,332.2 km^2 in 1985 and 26,332.3 km^2 in 2024. The independently documented vector watershed is 25,810.3 km^2, and its intersection with the terrestrial mask is 25,803.2 km^2 (Table S20). Because the original mapping boundary cannot be fully established from the inherited raster series, the 2.0% difference from the vector watershed is disclosed rather than removed by an arbitrary scaling factor. The combined Rivers, Lakes and Ocean class includes freshwater as well as potentially coastal cells; it does not measure the marine component separately. Table S23 reports an independent extraction for 1985 and 2024 on the terrestrial domain, which is distinct from the original forty-year series.

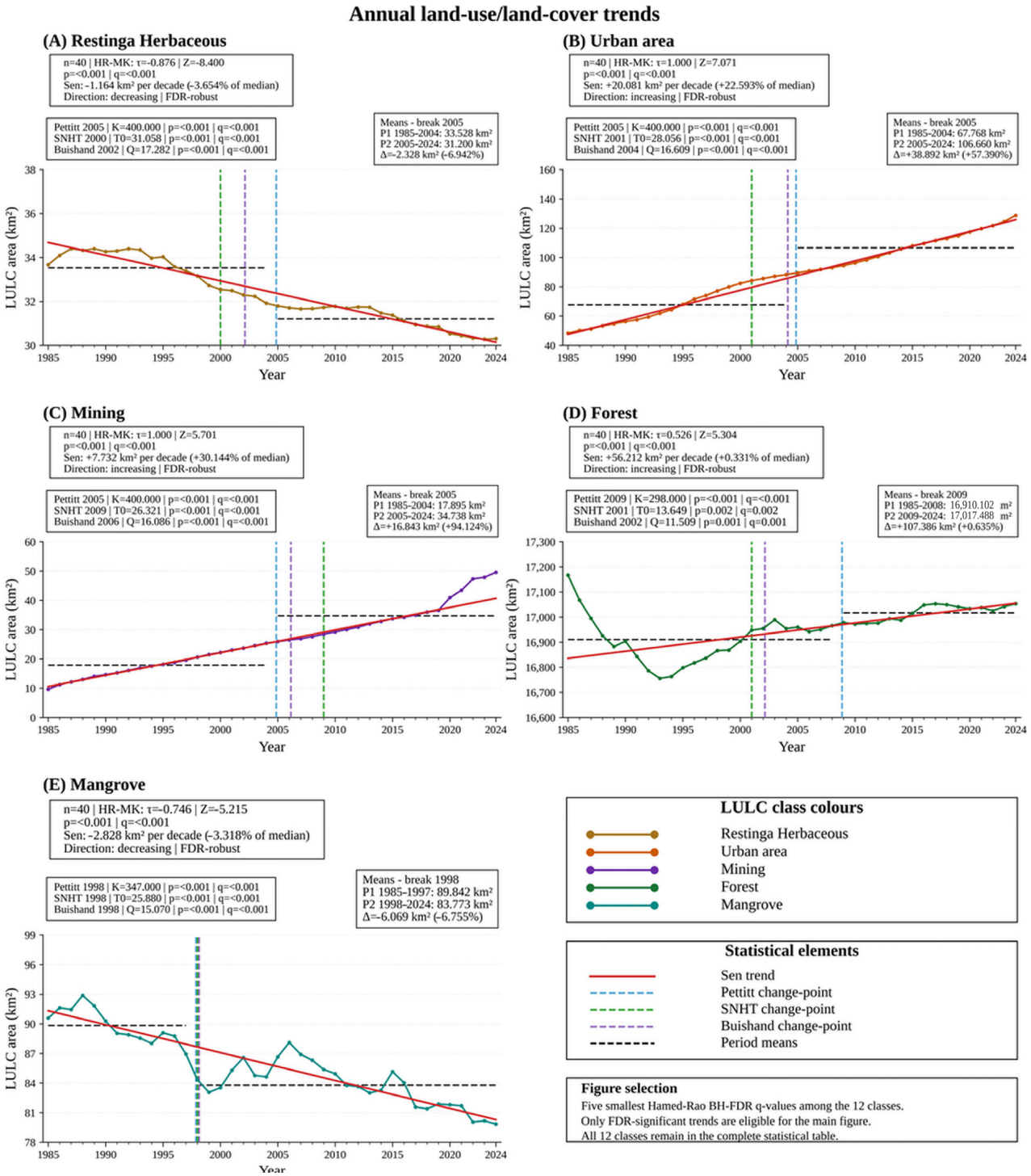


Figure 11. Annual trends in selected land-use and land-cover classes. (**A**) Restinga Herbaceous; (**B**) Urban area; (**C**) Mining; (**D**) Forest; (**E**) Mangrove. The full-series Sen lines are descriptive statistical summaries; Forest is non-monotonic and is interpreted using separate pre- and post-minimum trends in Table S15b. Strictly monotonic Urban area and Mining trajectories are emphasised descriptively.

Forest decreased from 17,166.5 km^2 in 1985 to 17,053.2 km^2 in 2024, a net change of −113.3 km^2 (−0.7%). Its minimum occurred in 1993 (16,755.3 km^2), followed by partial recovery. Agriculture/Pasture changed by +0.6%, while Mangrove and Restinga Herbaceous decreased by 11.9% and 10.0%, respectively (Table 4 and Table S15b). These class areas describe the original raster domain, not an independently reconciled estimate of total terrestrial catchment area.

Urban area expanded from 48.3 to 128.7 km^2 (+166.3%), and Mining from 9.6 to 49.5 km^2 (+415.5%). The large relative changes arise from small initial areas and should not be interpreted as equivalent to a basin-wide transformation. Other non-vegetated and composite Rivers, Lakes and Ocean classes declined on the original raster support (Table 4).

The selected LULC series exhibit contrasting temporal shapes (Figure 11). Although Forest has a positive full-period rank slope, its decline followed by recovery makes a single monotonic summary unsuitable. Urban area and Mining increase throughout the annual series; their observed area changes are more informative here than tests of perfect temporal ordering (Table S15b).

Urban area increased monotonically across the forty annual maps, from 48.3 to 128.7 km^2, and has Kendall τ = 1.000 and a global Sen slope of +20.1 km^2 decade^{-1} (Figure 11B). The strict sequence is a property of the mapped product, potentially influenced by temporal-consistency filtering, rather than independent proof of a physically irreversible land-cover trajectory (Table S15b).

Mining also increased monotonically (τ = 1.000; Sen +7.7 km^2 decade^{-1}; Figure 11C). As with Urban area, the consistent annual ordering and change in mapped extent are reported descriptively; formal probabilities are not interpreted as independent confirmation of continuous expansion in every location or year.

Restinga Herbaceous and Mangrove show decreasing monotonic tendencies (Sen −1.2 and −2.8 km^2 decade^{-1}, respectively; Figure 11A,E). Their mapped changes concern classified extent and should not be equated with independently measured ecological degradation.

Forest does not follow a monotonic course over 1985–2024. Classified area declined to 16,755.3 km^2 in 1993 and then partly recovered; descriptive Sen slopes are −459.4 km^2 decade^{-1} before that minimum and +77.8 km^2 decade^{-1} thereafter (Table S15b). The positive full-period Sen slope (+56.2 km^2 decade^{-1}) is misleading if interpreted as sustained expansion, because the 2024 area remains 113.3 km^2 below that of 1985. Mean-shift candidates dated 2001–2009 describe a different property of the series and should not be equated with the 1993 turning point (Figure 11D).

Urban expansion is consistent with documented landscape changes elsewhere along the São Paulo coast [67,68]. Mining growth is more spatially concentrated. The mapped reduction in Beach area requires a different interpretation because tidal circulation, waves and estuarine currents redistribute sediments within the Cananéia–Iguape system [69,70]. Changes in classified surface area may therefore reflect coastal dynamics and image-classification variability as well as persistent land-cover change.

3.4. Contributing-Area Validation and LULC-Discharge Associations

All ten DEM-delineated contributing areas satisfy the prespecified ±10% agreement criterion relative to official drainage areas (Table S14; Figure 12A,B). Differences are +1.2% at ID1-F, +1.0% at ID3-F and −9.4% at ID6-F. The alternative station polygons yield substantially larger discrepancies of +29.4%, −58.5% and −26.8%, respectively, demonstrating the sensitivity of geographical matching to boundary definition. The principal associations use the DEM-delineated areas and land-cover observations extracted within their boundaries for all forty years, without proportional area rescaling. The remaining discrepancy at ID6-F and the separate uncertainty in ID3-F station-code provenance limit the interpretation of area agreement as a complete validation of the hydrometric record.

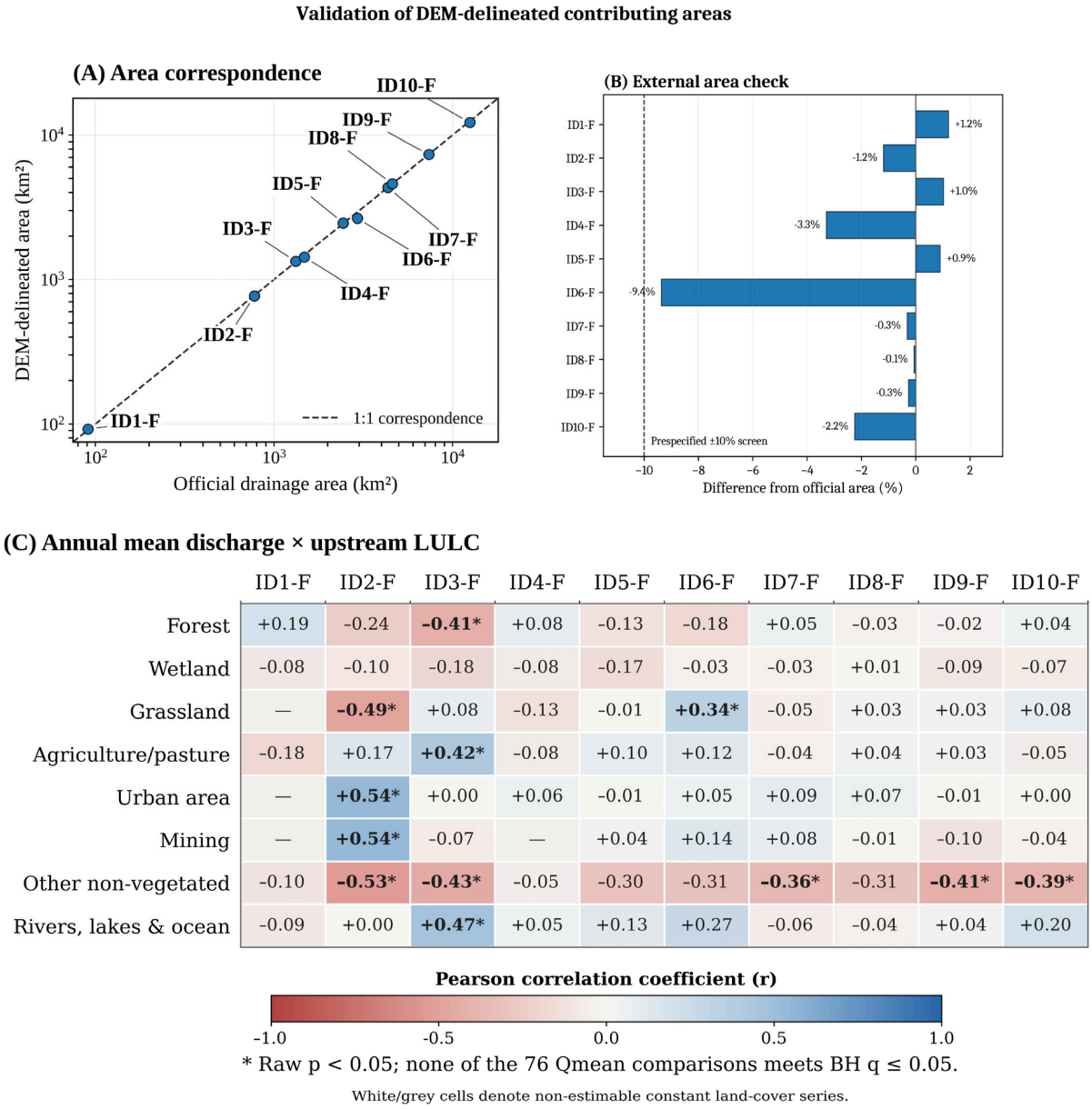


Figure 12. Validation of station contributing areas and contemporaneous mean-discharge associations. (**A**) DEM-delineated versus official drainage area, with a 1:1 reference; (**B**) percentage differences relative to official areas, with the −10% screening bound; (**C**) Pearson correlation coefficients between Q_{mean} and eight local MapBiomas land-cover percentages over 1985–2024. Asterisks indicate unadjusted $p < 0.05$; none of the 76 Q_{mean} coefficients survives within-metric BH correction (Table S21).

Spatial checks also examined gauge position, polygon topology, upstream nesting and raster coverage. The largest absolute raster–vector area difference across 480 domain–year evaluations was 0.016% (Table S14; Supplementary Data I). These results support internal consistency between the delineated polygons and the classified raster extraction. They do not establish that gauge metadata, discharge measurements or individual land-cover classes are free of error. Station-level areas, nesting diagnostics, annual classified areas and the complete coverage inventory are provided in Supplementary Data I.

The exploratory precipitation–LULC matrix remains in Supplementary Figure S2 because precipitation was represented by regional rain-gauge descriptors rather than rainfall observed over each contributing area. Those correlations describe temporal coincidence between spatially mismatched series; they neither measure a local land-cover response nor demonstrate that changes in land cover influenced precipitation (Tables S5 and S6).

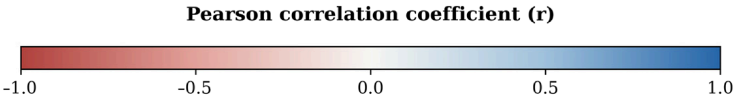
Of 240 planned contemporary Pearson comparisons between local land-cover percentages and discharge, 228 were estimable. Twenty-one had unadjusted $p < 0.05$: twelve for Q_{mean}, seven for Q_{min} and two for Q_{max}. None met $q \leq 0.05$ within the corresponding complete 76-test discharge family, and none met that threshold in the pooled 228-test analysis (Table S21). The full row-level coefficients, nominal p values and both q values are available in Supplementary Data I. The Q_{mean}, Q_{min} and Q_{max} matrices appear in Figures 12C and 13A,B. Nominally marked cells must not be read as adjusted evidence, and neither spatial matching nor BH correction eliminates possible temporal confounding.

(A) Minimum discharge and upstream land cover

	ID1-F	ID2-F	ID3-F	ID4-F	ID5-F	ID6-F	ID7-F	ID8-F	ID9-F	ID10-F
Forest	+0.16	-0.33	-0.31	-0.12	-0.31	+0.03	-0.20	+0.03	+0.01	+0.12
Wetland	+0.26	+0.01	-0.07	-0.12	-0.26	+0.05	-0.12	+0.02	-0.13	-0.04
Grassland	—	-0.16	+0.17	+0.07	**+0.33***	**+0.33***	+0.25	+0.10	-0.01	+0.14
Agriculture/pasture	-0.15	+0.28	+0.32	+0.12	+0.31	-0.08	+0.23	-0.04	+0.01	-0.14
Urban area	—	+0.28	-0.15	-0.09	-0.09	+0.05	-0.06	+0.07	-0.05	+0.00
Mining	—	+0.31	-0.23	—	-0.19	+0.12	-0.13	-0.03	-0.16	-0.06
Other non-vegetated	-0.08	**-0.50***	-0.29	-0.23	-0.29	-0.17	**-0.34***	-0.31	**-0.46***	**-0.34***
Rivers, lakes & ocean	-0.18	+0.36	**+0.52***	+0.16	+0.17	+0.24	-0.01	-0.17	+0.00	+0.14

(B) Maximum discharge and upstream land cover

	ID1-F	ID2-F	ID3-F	ID4-F	ID5-F	ID6-F	ID7-F	ID8-F	ID9-F	ID10-F
Forest	+0.14	**-0.38***	-0.31	+0.04	-0.24	-0.15	-0.01	+0.04	+0.02	+0.07
Wetland	-0.07	-0.14	+0.02	-0.07	-0.23	+0.08	-0.12	-0.08	-0.07	-0.09
Grassland	—	-0.19	+0.12	+0.13	+0.02	+0.17	+0.02	-0.08	-0.01	-0.01
Agriculture/pasture	-0.13	+0.33	+0.30	-0.04	+0.22	+0.08	+0.00	-0.03	-0.01	-0.07
Urban area	—	+0.26	+0.04	+0.03	-0.12	+0.16	+0.03	-0.04	-0.02	-0.00
Mining	—	+0.29	-0.02	—	-0.16	+0.24	-0.00	-0.07	-0.08	-0.01
Other non-vegetated	-0.10	-0.35	-0.27	-0.06	-0.01	+0.00	-0.30	-0.30	**-0.37***	-0.24
Rivers, lakes & ocean	-0.05	+0.08	+0.24	+0.04	+0.18	+0.02	+0.03	-0.02	-0.06	+0.08



* Unadjusted p < 0.05; no coefficient survives BH correction within its discharge-metric family.

An em dash (—) denotes a non-estimable coefficient (absent or constant land-cover class).

Figure 13. Contemporaneous Pearson correlations between upstream land-cover percentages and (**A**) annual minimum discharge (Q_{min}) and (**B**) annual maximum discharge (Q_{max}), 1985–2024, within ten DEM-delineated catchments. Red and blue indicate negative and positive coefficients, respectively. Asterisks indicate unadjusted $p < 0.05$; none of the 76 estimable comparisons in either metric family remains significant after BH adjustment at $q \leq 0.05$. Grey cells identify constant or absent classes for which a coefficient cannot be estimated. The Q_{mean} matrix appears in Figure 12C. Tables S21 and S22 summarise the results, and Supplementary Data I provides the complete coefficients, probabilities and sensitivity analyses. An em dash (—) in a grey cell indicates that the correlation is not estimable because the land-cover class is absent or constant; it does not represent a zero coefficient.

For ID3-F, the Rivers, Lakes and Ocean class is positively correlated with contemporaneous Q_{mean} (r = +0.471; n = 36) and Q_{min} (r = +0.523; n = 36), but the within-metric BH q values are 0.0765 and 0.0809, respectively (Table S22; Figures 12C and 13A). The association is therefore not FDR-robust in the primary specification. Detrended correlations attain adjusted significance under a different temporal model, whereas first differences do not; neither alternative independently substantiates an effect of mapped land cover on discharge. Changes in mapped surface-water area may also follow river stage. The coefficients should consequently be interpreted as contemporaneous correspondence rather than directional hydrological effects.

Record exclusions, alternative temporal windows and land-cover denominators were examined in separate sensitivity cases (Tables S17c,d, S21 and S22). The principal annual maps and Pearson matrices use the full discharge records, including ID1-F observations in 2020 and 2022 and the 2024 ID7-F Q_{min} value. Spatial correspondence is therefore evaluated independently of the influence of these observations. The absence of BH-supported contemporaneous associations, together with unresolved measurement and classification uncertainties, limits hydrological attribution at catchment scale.

4. Discussion

Across the basin, precipitation shows a clearer spatial concentration of significant annual trends than streamflow, but the two monitoring networks do not provide spatially equivalent measures of the water balance. Rainfall is summarised from a regional gauge network, whereas discharge integrates processes within individual and partly nested contributing areas. The contrast between Figures 5 and 9 is therefore interpreted as a difference in observed hydroclimatic trajectories rather than as a quantified precipitation–runoff residual, with dependence, seasonal and interstation diagnostics used to qualify persistence and timing without assigning a common cause.

4.1. Hydroclimatic Trends and Streamflow Variability

The strongest positive rainfall trends occur at neighbouring Paraná gauges where the series also contain marked interstation consistency departures around 1981. At ID13-R, the median station/reference ratio increases by 41.4%, and at ID14-R by 34.2%, while the corresponding changes in double-mass slope are 40.8% and 44.0% (Table S13b). A shared climatic contribution cannot be excluded, but neither can changes in station operation, daily aggregation, instrumentation or processing. The origin and homogeneity of these records cannot be settled from the monthly aggregates alone, especially as the distinction between ANA bruto and consistido data is undocumented. The AR(1) null must also be interpreted with care: estimated persistence falls after detrending or segment demeaning, and the adjusted support for an abrupt change depends on that choice (Table S10d). The network therefore supports spatially heterogeneous rainfall trends, not an unqualified inference of climatic intensification at every gauge.

Regional climatic evidence remains heterogeneous. Observational studies have identified changes in climate extremes in eastern Paraná [71], while Varuolo-Clarke et al. [72] reported that summer-rainfall increases across southeastern South America exceed those reproduced by many climate models. Subsequent analysis connected part of this regional change to stronger moisture transport by the South American low-level jet [73]. Within the Ribeira Basin, the decrease at Serrana do Sul and the absence of spatially coincident change points caution against treating the network as a single uniform trend. These regional patterns are considered alongside studies of southeastern Brazilian rainfall extremes and combined satellite–gauge records [74,75] and the role of circulation, relief and geography in South American precipitation [76–78].

The annual streamflow results differ by discharge metric. At ID5-F, decreasing Q_{max} at Juquiá is the only HR-MK result surviving within-variable BH adjustment (Figure 9), although the alternative HAC linear formulation is less decisive (Tables S7 and S8). The three nominal positive results at Jacupiranga Q_{mean} and Q_{min} and Balsa do Cerro Azul Q_{max} do not meet the adjusted trend criterion. Separate classical change-point analyses identify a 1993 candidate for Jacupiranga Q_{mean}, supported by all three tests, and Q_{min} candidates at Juquiá and Balsa do Cerro Azul supported by Buishand alone; no Q_{max} candidate survives BH adjustment (Table S3). These distinctions matter because a monotonic trend, a difference between segment means and an operationally caused regime shift are not interchangeable claims. The +33.3% Jacupiranga Q_{mean} contrast has some complementary seasonal and HAC support but is weakened under the full-record AR(1) null, while the longest uninterrupted subrecord does not extend across 1993 (Tables S9 and S10d). Its precise timing cannot be treated as independently verified. Differences among flow metrics are consistent with the distinct influences of climatic variability, catchment storage, land use and water management on discharge magnitude and timing [79–81].

A water-balance interpretation places these discharge contrasts within the partitioning of precipitation among runoff, evapotranspiration and storage, together with withdrawals or transfers where present. Atlantic Forest modelling indicates how climatic and land-cover changes can alter infiltration, evapotranspiration and water yield [82], but quantitative Budyko or elasticity attribution would require catchment rainfall and evapotranspiration observations unavailable here. Storm duration, antecedent moisture and catchment characteristics can also separate rainfall-intensity changes from flood responses [83]. Jacupiranga's winter increases thus identify a seasonal feature of the discharge record without isolating a change in recharge, baseflow or water management.

Divergent precipitation and streamflow trajectories have been documented in other basins. Chen et al. [84] evaluated declining Huangfuchuan discharge in relation to climatic variability and human activity, whereas São Paulo studies also reported discharge changes not accompanied by equivalent precipitation trends [6–8]. The Juquiá hydropower complex and its water-transfer context are described in regional and operator sources [85,86]. Broader assessments document how impoundments may alter tropical river hydromorphology and flood dynamics [87,88], and scenario-based modelling illustrates the sensitivity of water availability and extremes in an Atlantic Forest catchment [89]. These studies indicate plausible pathways, but none demonstrates the cause of the changes observed at the Ribeira gauges.

Operational history is relevant to interpreting the Juquiá River, but it does not supply a measured explanation for the observed trends. The França, Fumaça, Alecrim, Serraria, Porto Raso and Barra hydropower plants entered operation in 1958, 1964, 1974, 1978, 1982 and 1986, respectively [24] (see Supplementary Figure S1). The São Lourenço supply system is authorised to withdraw up to 6.4 $m^3\ s^{-1}$ from the Cachoeira do França reservoir under a 2016 authorisation; water-supply operation was reported in 2018 [90,91]. Neither installed capacity nor licenced abstraction is a series of actual reservoir releases or withdrawn volumes. For 48 common years in 1970–2023, Q_{max} Sen slopes at upstream ID5-F and downstream ID7-F were -15.4 and $-0.3\ m^3\ s^{-1}$ $decade^{-1}$, respectively, despite positive interstation covariation (Table S19b). The downstream gauge integrates a substantially larger catchment, so tributary inputs, hydrological storage, record differences and operating conditions could all contribute to the mismatch. The available evidence does not isolate any one of these mechanisms.

Interstation discharge diagnostics reveal relative differences that do not independently identify hydrometric interventions. The Juquiá Q_{max} decline at ID5-F is accompanied by a weaker response at downstream ID7-F, despite positive co-variation between the common-period records. These observations are compatible with several climatic, spatial,

operational or measurement-related influences. Ratings, releases and withdrawal histories would be needed to evaluate the individual contributions (Tables S13 and S19b; Figure S3).

4.2. Land-Use and Land-Cover Changes and Coastal Environments

The Forest series should not be interpreted as a simple recovery trend. The sharp early loss, 1993 minimum and subsequent increase yield a positive full-series Sen slope even though the 1985–2024 endpoint difference is negative (Table S15b). Reported changes in forest extent may reflect conversion, regrowth and classification consistency, but annual class area alone cannot distinguish forest age, structure or ecological quality [92,93].

The small net change in forest extent likewise leaves its hydrological implications open. Caballero et al. [94] describe changes in surface–atmosphere water and energy exchanges following Brazilian land-cover conversion, with responses depending on biome and climate. Atlantic Forest modelling also indicates that greater forest cover can enhance infiltration and reduce surface runoff without necessarily increasing annual water yield [82], so the partial recovery in Ribeira need not correspond to a single direction of change in mean or extreme discharge.

Urban area and Mining expanded substantially from small initial areas, and their annual mapped series are strictly increasing. Temporal-consistency filters in annual MapBiomas products may contribute to this ordering; therefore, $\tau = 1.000$ is reported as a property of these classified trajectories rather than as independent evidence of physically monotonic land conversion. Their potential hydrological relevance remains dependent on location, connectivity and catchment scale.

Mangrove and herbaceous-restinga losses occur in environments where estuarine, sedimentary and continental influences interact, making their separation from annual class areas difficult. Physical setting and land-use history have been associated with Atlantic Forest hydrological responses [95], and climatic variability is documented in the Cananéia–Iguape system [57]. Analyses of wetlands and built surfaces in the uMngeni catchment further illustrate the dependence of mapped change on spatial scale [96], but these comparisons do not determine the mechanisms underlying the Ribeira trajectories.

The 31.8% decline in Beach area describes a reduction in classified surface extent, not a measured rate of coastal erosion. Tides and estuarine currents influence sediment redistribution in the Cananéia region [69], and depositional mobility is documented for Cardoso Island [70]. These processes, combined with classification uncertainty for narrow and dynamic surfaces, preclude interpretation as shoreline retreat without independent shoreline and sediment observations.

Potential land-cover effects on discharge depend on the extent, arrangement and hydrological connectivity of landscape change within the upstream area [97,98]. Matching annual land-cover observations to DEM-delineated catchments establishes a physically relevant spatial basis for comparison, but does not identify the direction or magnitude of a causal effect. None of the 228 estimable primary associations remains significant after within-metric BH adjustment (Figures 12C and 13; Table S21). Hydrological explanations must also account for catchment precipitation, storage, water withdrawals and uncertainty in the land-cover and discharge records.

4.3. Spatial Support, Scale and Exploratory Associations

The regional precipitation–land-cover comparison and the catchment-specific discharge analysis answer different spatial questions. Network precipitation descriptors cannot be interpreted as rainfall integrated over each upstream area, and their associations with basin-scale mapped classes remain exploratory (Figure S2). The local discharge matrices in Figures 12C and 13A,B use land-cover percentages from the contributing area of each

gauge. Although 21 of 228 estimable Pearson coefficients meet the unadjusted 5% threshold, none remains significant within its complete 76-test metric family after BH adjustment. The observed coefficient pattern therefore does not establish a common land-cover control on streamflow (Tables S21 and S22).

The ID3-F water-class associations illustrate the distinction between spatial matching and inferential support. Within its DEM-delineated catchment, correlations with Q_{mean} and Q_{min} are +0.471 and +0.523, respectively; both meet the nominal threshold, but neither satisfies $q \leq 0.05$ within its full metric family. Detrended relationships retain stronger adjusted evidence, whereas first differences do not (Table S22). These specifications describe different temporal components and cannot be combined as corroborating tests of a single mechanism. Moreover, the mapped Rivers, Lakes and Ocean class can vary with river stage or reservoir level. The available observations do not resolve the direction of influence between mapped water extent and discharge.

Geometric validation showed that all ten independently derived catchments are within $\pm 10\%$ of official drainage areas, although the -9.4% discrepancy at ID6-F remains close to the screening threshold (Figure 12). The raster–vector comparison and 40-year MapBiomas extraction support the validity of spatial matching, but do not eliminate station-record uncertainty, classification error or confounding in the statistical associations (Tables S14 and S21).

Catchment land-cover percentages use the total valid classified area as their principal denominator. Results based on the sum of the eight selected classes, alternative temporal windows and alternative station polygons are documented separately to distinguish denominator, temporal and spatial-support effects. Supplementary Data I contains the annual catchment areas and all 240 planned primary correlation records, with sample sizes, nominal probabilities and both BH adjustments. Table S21 summarises the complete testing families, while Table S22 examines ID3-F. Estimates derived from different spatial supports are not pooled or interpreted as measurements of the same catchment-level association.

The large ID1-F observations in 2020 and 2022, and the low 2024 ID7-F Q_{min} observation, warrant direct source-record checks. The values of 4.26 and 5.52 at ID1-F compare discharge-derived annual runoff depth with regional, not local catchment-integrated, rainfall (Table S17b). Excluding 2020 and 2022 strengthens the ID1-F Q_{max} Sen slope from -0.9 to -2.3 m^3 s^{-1} $decade^{-1}$, but the adjusted probability remains $q = 0.143$. The screened ID7-F Q_{min} slope also remains non-significant after BH adjustment (Table S17c). These analyses show that the principal inference does not depend on labelling the questioned records as erroneous, while leaving the original measurements and the unusually large segment contrasts explicitly unverified.

Spatially differentiated precipitation and discharge trajectories are compatible with several climatic, storage-related, landscape and water-management influences. The observational design does not separate their causal contributions. Catchment delineation and annual land-cover extraction establish geographical correspondence, while mechanistic assessment would additionally require catchment precipitation and evapotranspiration, verified hydrometric metadata, and reservoir-release or abstraction records [82,98,99].

4.4. Limitations and Future Perspectives

The station records differ in temporal coverage and completeness, and some lack metadata sufficient to establish rating-curve histories, the ANA precipitation processing category and the treatment of missing daily values. Relative-consistency diagnostics identify departures among records without determining whether they reflect observational changes or local climatic variability. AR(1) sensitivities depend on persistence estimation, and moving-block analyses may concern uninterrupted subrecords that exclude the candidate year. The basin-scale LULC trajectories also represent a raster domain of approximately

26,332 km^2. Class-by-class extraction within the documented terrestrial boundary covers the 1985 and 2024 endpoints, not a boundary-harmonised forty-year regional sequence (Tables S20–S23). These distinctions restrict temporal and spatial comparability and are evaluated through the separate diagnostics in Tables S7–S10d, S13b and S17b–d.

Regional precipitation indices and station discharge summaries do not constitute spatially matched water-balance components. Several discharge gauges drain nested areas and have unequal record completeness. Within the DEM-delineated catchments, none of the contemporaneous land-cover–discharge coefficients survives the specified BH adjustment. This finding limits evidence for an annual linear association; it does not demonstrate the absence of landscape-related hydrological effects. Interpretation remains conditional on serial dependence, catchment nesting, observational quality, classification uncertainty and unmeasured drivers. Studies of soil-water storage [100] and climate-land-cover interactions [101] illustrate why temporal correspondence alone cannot identify the underlying mechanisms.

MapBiomas classification uncertainty is particularly relevant for small or spatially dynamic classes. Forest follows a non-monotonic trajectory, whereas temporal-consistency filters may contribute to the strictly increasing Urban area and Mining series (Table S15b). The catchment geometries meet the area, topology and nesting criteria, although ID6-F differs from its official drainage area by −9.4%, close to the tolerance limit. Consistent raster coverage across forty annual maps supports geographical comparability without guaranteeing error-free land-cover classification or hydrometric observations (Tables S14 and S21–S23; Figure 12).

Commissioning dates, licenced withdrawals and the common-period ID5-F/ID7-F comparison constrain possible operational interpretations but are not substitutes for time series of reservoir releases, abstractions and local rainfall. Inferences about hydropower or transfer impacts remain hypotheses rather than established explanations for the observed streamflow patterns.

5. Conclusions

Annual precipitation trends are predominantly positive, but not uniform across the Ribeira de Iguape Basin: seven stations retain increasing and one a decreasing trend after BH adjustment. The exceptionally large positive changes and 1981 candidates at two neighbouring Paraná gauges coincide with departures from interstation reference series. Because station metadata and daily aggregation histories remain incomplete, these observations cannot be interpreted unequivocally as climatic discontinuities. The other precipitation candidates are likewise sensitive to dependence assumptions and, in some cases, short record segments.

Discharge changes are more localised. The declining annual maximum flow at Juquiá is the only streamflow trend that survives the prespecified BH adjustment, and the same magnitude of decline is not observed at the downstream station during common years. The targeted exclusions of the anomalous ID1-F observations and the isolated 2024 ID7-F minimum do not add any adjusted annual discharge trend. Statistical contrasts and the chronology of water infrastructure do not, on their own, identify an operative cause for the observed changes.

Urban and mining areas expanded during 1985–2024, whereas Forest reached a minimum in 1993 and recovered partially without regaining its 1985 extent. Land-cover observations within ten DEM-delineated catchments yielded 228 estimable contemporaneous discharge correlations. Twenty-one were nominally significant, but none remained significant after adjustment within its complete metric family. The evidence thus supports spatially contrasting precipitation, discharge and landscape trajectories, while leaving the causal contribution of land-cover change to river flow unresolved.

Supplementary Materials: The following supporting information can be downloaded at: https://www.mdpi.com/article/10.3390/earth7060185/s1, Supplementary Material I provides station inventories and annual estimates (Tables S1–S4), spatial-support and estimator comparisons (Tables S5, S6 and S11a–c), temporal and seasonal sensitivities (Tables S7–S10d), network-weighting analyses (Tables S12 and S18), interstation and catchment diagnostics (Tables S13 and S14), land-cover and hydrometric assessments (Tables S15–S20), and catchment-specific associations and spatial-domain comparisons (Tables S21–S23). Supplementary Figure S2 presents the exploratory regional precipitation–LULC matrix. The local Q_{mean}, Q_{min} and Q_{max} matrices appear in Figures 12C and 13A,B. Supplementary Data I contains all 240 planned primary comparisons, annual catchment-specific class areas for 1985–2024, spatial coverage diagnostics and record-exclusion sensitivities. Analytical code and source material are archived at https://doi.org/10.5281/zenodo.23583929. References [24,47,51–53,86,90,102–104] are cited in Supplementary Material I.

Author Contributions: Conceptualization, V.M.E. and E.G.; methodology, V.M.E.; software, V.M.E.; validation, V.M.E., J.B., N.G.B.d.L., P.M.d.B.T. and E.G.; formal analysis, V.M.E.; investigation, V.M.E.; resources, E.G.; data curation, V.M.E.; writing—original draft preparation, V.M.E.; writing—review and editing, J.B., N.G.B.d.L., P.M.d.B.T. and E.G.; visualisation, V.M.E.; supervision, E.G. All authors have read and agreed to the published version of the manuscript.

Funding: The first author was supported by the Coordination for the Improvement of Higher Education Personnel (CAPES) through a fellowship from the Social Demand Programme (DS-CAPES), Finance Code 001. The second author was supported by the São Paulo Research Foundation (FAPESP) through a Postdoctoral Fellowship, Grant No. 22/02383-3. The fourth author was supported by the National Council for Scientific and Technological Development (CNPq) through a Research Productivity Fellowship, Grant No. 304973/2017-3. The fifth author was supported by the São Paulo Research Foundation (FAPESP), Process No. 2024/19822-5, through the New Generation of Researchers Programme ("Projeto Geração", 2024). The funders had no role in the design of the study; in the collection, analyses, or interpretation of data; in the writing of the manuscript; or in the decision to publish the results.

Data Availability Statement: Precipitation and discharge records were obtained from ANA and São Paulo State agencies, and annual land-cover maps from MapBiomas Collection 10. Analytical code and source material are archived at https://doi.org/10.5281/zenodo.23583929. Supplementary Data I provides station-level land-cover areas for 1985–2024, catchment-validation and raster-coverage diagnostics, all planned primary correlations with nominal and BH-adjusted probabilities, and the corresponding sensitivity analyses. The terrestrial-basin class comparison covers the 1985 and 2024 endpoints. No additional primary observations were collected. The available metadata do not fully establish the ANA bruto/consistido category, daily-completeness rules underlying some monthly rainfall totals, or the measurement basis of the monthly discharge extrema.

Conflicts of Interest: The authors declare no conflicts of interest.

Abbreviations

The following abbreviations are used in this manuscript:

ANA	National Water and Basic Sanitation Agency
AR(1)	First-order autoregressive process
BH	Benjamini–Hochberg procedure
DAEE	São Paulo State Department of Water and Electric Energy
DEM	Digital elevation model
FDR	False discovery rate
HAC	Heteroskedasticity- and autocorrelation-consistent covariance
HR-MK	Hamed–Rao modified Mann–Kendall test
IBGE	Brazilian Institute of Geography and Statistics
LULC	Land use and land cover
Q_{mean}	Mean discharge

Q_{max}	Maximum discharge
Q_{min}	Minimum discharge
SACZ	South Atlantic Convergence Zone
SNHT	Standard Normal Homogeneity Test
SP-Águas	São Paulo State Water Agency
CBH-RB	Ribeira de Iguape River Basin Committee

References

1. Tucci, C.; Clarke, R. Impactos das mudanças da cobertura vegetal no escoamento: Revisão. *Rev. Bras. Recur. Hidr.* **1997**, *2*, 135–152. [CrossRef]
2. Botelho, R.G.M.; Silva, A.S. Bacia hidrográfica e qualidade ambiental. In *Reflexões Sobre a Geografia Física no Brasil*; Vitte, A.C., Guerra, A.J.T., Eds.; Bertrand Brasil: Rio de Janeiro, Brazil, 2004.
3. Agência Nacional de Águas. *Hidrologia: Conceitos Básicos e Aplicações*; ANA: Brasília, Brazil, 2011.
4. Ross, J.L.S. *Ecogeografia do Brasil: Subsídios Para Planejamento Ambiental*; Oficina de Textos: São Paulo, Brazil, 2006.
5. dos Santos, B.C.; de Souza, P.H.; Sanches, R.G.; Bolleli, T.d.M.; Tech, A.R.B. O efeito do planalto ocidental paulista na variabilidade e nos anos extremos das chuvas no período de 1979–2019. *Cad. Geogr.* **2021**, *31*, 168. [CrossRef]
6. Uliana, E.M.; Silva, D.D.; Uliana, E.M.; Rodrigues, B.S.; Corrêdo, L.P. Análise de tendência em séries históricas de vazão e precipitação: Uso de teste estatístico não paramétrico. *Ambiente Água* **2015**, *10*, 82–88. [CrossRef]
7. Moraes, J.M.; Genovez, A.M.; Mortatti, J.; Ballester, M.V.; Krusch, A.V.; Martinelli, L.A.; Victoria, R.L. Análise de intervenção das séries temporais de vazão dos principais rios da bacia do rio Piracicaba. *Rev. Bras. Recur. Hidr.* **1997**, *2*, 65–79. [CrossRef]
8. Groppo, J.D.; Moraes, J.M.; Beduschi, C.E.; Martinelli, L.A. Análise de séries temporais de vazão e precipitação em algumas bacias do Estado de São Paulo com diferentes graus de intervenções antrópicas. *Geociências* **2005**, *24*, 181–193. Available online: https://www.revistageociencias.com.br/geociencias-arquivos/24_2/Artigo%206.pdf (accessed on 21 October 2026).
9. Vilanova, M.R.N. Trends in mean annual streamflows in Serra da Mantiqueira environmental protection area. *Braz. Arch. Biol. Technol.* **2014**, *57*, 1004–1012. [CrossRef]
10. Capozzoli, C.R.; Cardoso, A.d.O.; Ferraz, S.E.T. Padrões de variabilidade de vazão de rios nas principais bacias brasileiras e associação com índices climáticos. *Rev. Bras. Meteorol.* **2017**, *32*, 243–254. [CrossRef]
11. Lee, D.; Ward, P.J.; Block, P. Identification of symmetric and asymmetric responses in seasonal streamflow globally to ENSO phase. *Environ. Res. Lett.* **2018**, *13*, 044031. [CrossRef]
12. Limberger, L.; Silva, M.E.S. Teleconexões atmosféricas e vazão fluvial na Bacia Amazônica Brasileira por meio de mapas de correlação linear. *Entre-Lugar* **2021**, *12*, 244–268. [CrossRef]
13. Tiezzi, R.O. Variabilidade Hidroclimatológica e Seus Efeitos no Suprimento de Energia Elétrica do Sistema Interligado Nacional. Ph.D. Thesis, Universidade Estadual de Campinas, Campinas, Brazil, 2015.
14. Zuo, D.; Xu, Z.; Wu, W.; Zhao, J.; Zhao, F. Identification of streamflow response to climate change and human activities in the Wei River basin, China. *Water Resour. Manag.* **2014**, *28*, 833–851. [CrossRef]
15. Menezes, J.P.C.; Franco, C.S.; De Oliveira, L.F.C.; Bittencourt, R.P.; Farias, M.d.S.; Fia, R. Morfometria e evolução do uso do solo e da vazão de máxima em uma micro bacia urbana. *Rev. Bras. Geomorfol.* **2014**, *15*, 659–672. [CrossRef]
16. de Sousa, R.G.; Martins, L.; Nunes, F.S.; Silva, F.B. Análise da precipitação, vazão, uso e cobertura da terra na bacia do rio São João/MG. *Rev. Augustus* **2019**, *24*, 146–154. [CrossRef]
17. Souza, J.C.; Martins, P.T.A.; Druciaki, V.P. Uso e cobertura do solo no Cerrado: Panorama do período de 1985 a 2018. *Élisée Rev. Geogr. UEG* **2020**, *9*, e922020. Available online: https://www.revista.ueg.br/index.php/elisee/article/view/10857 (accessed on 21 October 2026).
18. Xavier, R.L.; Menezes, D.B.; Silva, F.L.d. Mapeamento de uso e ocupação do solo utilizando dados do MapBiomas: Uma abordagem manual para aumento de precisão aplicada em Meridiano, São Paulo. *Rev. Bras. Geogr. Fis.* **2024**, *17*, 1992–2007. [CrossRef]
19. Jiang, C.; Zhang, L.; Tang, Z. Multi-temporal scale changes of streamflow and sediment discharge in the headwaters of Yellow River and Yangtze River on the Tibetan Plateau, China. *Ecol. Eng.* **2017**, *102*, 240–254. [CrossRef]
20. de Bodas Terassi, P.M.; Baratto, J.; Biffi, V.H.R.; Galvani, E.; de Gois, G.; Flores, D.M.; da Silva Scheer, M.A.P.; Sobral, B.S.; Cuevas, J. Warming, rainfall extremes, and land use change in the Iguaçu Triple Frontier, South America. *Earth Syst. Environ.* **2026**, *10*, 8241–8261. [CrossRef]
21. Cotrim, M.E.B. Avaliação da Qualidade da Água na Bacia Hidrográfica do Ribeira de Iguape com Vistas ao Abastecimento Público. Ph.D. Thesis, Instituto de Pesquisas Energéticas e Nucleares, São Paulo, Brazil, 2006.

22. Cunha-Lignon, M.; Coelho, C., Jr.; Almeida, R.; Menghini, R.P.; Schaeffer-Novelli, Y.; Cintrón, G.; Dahdouh-Guebas, F. Characterisation of mangrove forest types in view of conservation and management: A review of mangals at the Cananéia region, São Paulo State, Brazil. *J. Coast. Res.* **2011**, *64*, 349–353.
23. Prado, H.M.; Schlindwein, M.N.; Murrieta, R.S.S.; Nascimento, D.R.; de Souza, E.P.; Cunha-Lignon, M.; Mahiques, M.M.; Giannini, P.C.F.; Contente, R.F. The Valo Grande channel in the Cananéia-Iguape estuary-lagoon complex (SP, Brazil): Environmental history, ecology, and future perspectives. *Ambiente Soc.* **2019**, *22*, e01822. [CrossRef]
24. Sistema Integrado de Gerenciamento de Recursos Hídricos do Estado de São Paulo (SIGRH). Plano Estadual de Recursos Hídricos 2004/2007: Relatório Síntese, Chapter 4.4. Available online: https://sigrh.sp.gov.br/public/uploads/documents/6962/cap_04_04.pdf (accessed on 21 October 2026).
25. Comitê da Bacia Hidrográfica do Ribeira de Iguape e Litoral Sul (CBH-RB). *Bacia Hidrográfica do Ribeira de Iguape e Litoral Sul: Ano-Base 2016*; CBH-RB: Registro, Brazil, 2016.
26. Ross, J.L.S. Ribeira do Iguape basin morphogenesis and the environmental systems. *GEOUSP Espaç. E Tempo* **2002**, *6*, 21–46. [CrossRef]
27. Nunes, L.H.; Koga-Vicente, A.; Candido, D.H. Clima da região Sudeste do Brasil. In *Tempo e Clima no Brasil*; Oficina de Textos: São Paulo, Brazil, 2015.
28. Alvares, C.A.; Stape, J.L.; Sentelhas, P.C.; de Moraes Gonçalves, J.L.; Sparovek, G. Köppen's climate classification map for Brazil. *Meteorol. Z.* **2013**, *22*, 711–728. [CrossRef]
29. Beck, H.E.; Zimmermann, N.E.; McVicar, T.R.; Vergopolan, N.; Berg, A.; Wood, E.F. Present and future Köppen-Geiger climate classification maps at 1-km resolution. *Sci. Data* **2018**, *5*, 180214, Correction in *Sci. Data* **2020**, *7*, 274. [CrossRef] [PubMed]
30. Galvani, E.; Emiliano, V.M.; Baratto, J. Comparação dos principais sistemas de classificação climática aplicados à bacia hidrográfica do Ribeira de Iguape. In *Climas do Brasil: Classificação Climática e Aplicações*; Novais, G.T., Ed.; Totalbooks: Porto Alegre, Brazil, 2023.
31. Reboita, M.S.; Krusche, N.; Ambrizzi, T.; Rocha, R.P.d. Entendendo o tempo e o clima na América do Sul. *Terrae Didat.* **2012**, *8*, 34–50. [CrossRef]
32. Diegues, A.C. *O Mito Moderno da Natureza Intocada*, 4th ed.; Hucitec: São Paulo, Brazil, 2002.
33. Companhia Ambiental do Estado de São Paulo. *Relatório de Qualidade das Águas Interiores do Estado de São Paulo*; CETESB: São Paulo, Brazil, 1998.
34. Chiodi, R.E.; de Almeida, G.F.; de Assis, L.H.B. O mercado convencional da banana: Sujeição da agricultura familiar no Vale do Ribeira-SP. *Desenvolv. EM Quest.* **2020**, *18*, 146–165. [CrossRef]
35. Silva Júnior, J.A. Desafios e perspectivas do Programa Territórios da Cidadania: O caso do Território da Cidadania Vale do Ribeira. Ph.D. Thesis, Universidade de São Paulo, São Paulo, Brazil, 2015.
36. Chow, V.T.; Maidment, D.R.; Mays, L.W. *Applied Hydrology*; McGraw-Hill: New York, NY, USA, 1988; ISBN 007-010810-2.
37. Departamento de Águas e Energia Elétrica (DAEE). Rede Hidrológica Básica do Estado de São Paulo: Telemetria via Satélite. Available online: https://www.saisp.br/site/Rede_Basica_DAEE.html (accessed on 21 October 2026).
38. MapBiomas. Brazilian Land Cover and Use Map Series, Collection 10: Legend Codes. Available online: https://brasil.mapbiomas.org/wp-content/uploads/sites/4/2025/08/Legenda-Colecao-10-Legend-Code.pdf (accessed on 21 October 2026).
39. Oliveira, N.F.; Arraut, E.M. A evolução da acurácia das coleções do MapBiomas para a paisagem altamente fragmentada de São Paulo. *Rev. Bras. Cartogr.* **2024**, *76*. [CrossRef]
40. MapBiomas. Brazilian Land Cover and Use Map Series, Collection 8. 2023. Available online: https://brasil.mapbiomas.org/ (accessed on 21 October 2026).
41. Instituto Brasileiro de Geografia e Estatística (IBGE). *Monitoramento da Cobertura e Uso da Terra do Brasil: 2018/2020*; IBGE: Rio de Janeiro, Brazil, 2022.
42. De Souza, V. Análise Multitemporal das Perdas de solo por Erosão Laminar e do Regime de Vazão Fluvial na Bacia do rio Jacaré Guaçú (SP). Ph.D. Thesis, Faculdade de Filosofia, Letras e Ciências Humanas, São Paulo, Brazil, 2016.
43. Tucci, C.E.M. (Ed.) *Hidrologia: Ciência e Aplicação*, 3rd ed.; Editora da UFRGS/ABRH: Porto Alegre, Brazil, 2004.
44. World Meteorological Organization. *Guide to Hydrological Practices, Volume I: Hydrology—From Measurement to Hydrological Information*; WMO: Geneva, Switzerland, 2008.
45. Sankarasubramanian, A.; Vogel, R.M. Annual hydroclimatology of the United States. *Water Resour. Res.* **2002**, *38*, 19-1–19-12. [CrossRef]
46. Mann, H.B. Nonparametric tests against trend. *Econometrica* **1945**, *13*, 245–259. [CrossRef]
47. Hamed, K.H.; Ramachandra Rao, A. A modified Mann-Kendall trend test for autocorrelated data. *J. Hydrol.* **1998**, *204*, 182–196. [CrossRef]
48. Yue, S.; Pilon, P.; Phinney, B.; Cavadias, G. The influence of autocorrelation on the ability to detect trend in hydrological series. *Hydrol. Process.* **2002**, *16*, 1807–1829. [CrossRef]
49. Kendall, M.G. *Rank Correlation Methods*, 4th ed.; Charles Griffin: London, UK, 1975.
50. Sen, P.K. Estimates of the regression coefficient based on Kendall's tau. *J. Am. Stat. Assoc.* **1968**, *63*, 1379–1389. [CrossRef]

51. Benjamini, Y.; Hochberg, Y. Controlling the false discovery rate: A practical and powerful approach to multiple testing. *J. R. Stat. Soc. Ser. B* **1995**, *57*, 289–300. [CrossRef]
52. Newey, W.K.; West, K.D. A simple, positive semi-definite, heteroskedasticity and autocorrelation consistent covariance matrix. *Econometrica* **1987**, *55*, 703–708. [CrossRef]
53. Künsch, H.R. The jackknife and the bootstrap for general stationary observations. *Ann. Stat.* **1989**, *17*, 1217–1241. [CrossRef]
54. Pettitt, A.N. A non-parametric approach to the change-point problem. *Appl. Stat.* **1979**, *28*, 126–135. [CrossRef] [PubMed]
55. Alexandersson, H. A homogeneity test applied to precipitation data. *J. Climatol.* **1986**, *6*, 661–675. [CrossRef]
56. Buishand, T.A. Some methods for testing the homogeneity of rainfall records. *J. Hydrol.* **1982**, *58*, 11–27. [CrossRef]
57. Baratto, J.; de Bodas Terassi, P.M.; de Beserra de Lima, N.G.; Galvani, E. Precipitation anomalies and trends estimated via satellite rainfall products in the Cananeia–Iguape coastal system, southeast region of Brazil. *Climate* **2024**, *12*, 22. [CrossRef]
58. Tozato, H.d.C.; Dubreuil, V.; de Mello-Théry, N.A. Tendências e rupturas climato-hidrológicas no sitio Ramsar PARNA Pantanal (MT, Brasil). *Rev. Bras. Climatol.* **2014**, *13*. [CrossRef]
59. Sagarika, S.; Kalra, A.; Ahmad, S. Evaluating the effect of persistence on long-term trends and analyzing step changes in streamflows of the continental United States. *J. Hydrol.* **2014**, *517*, 36–53. [CrossRef]
60. Departamento de Águas e Energia Elétrica (DAEE). *Plano Estadual de Recursos Hídricos: Relatório da Bacia do Ribeira de Iguape*; DAEE: São Paulo, Brazil, 1999.
61. Limberger, L. Estudos de teleconexões atmosféricas e possibilidades de avanços na climatologia geográfica: Conceitos, fontes de dados e técnicas. *Rev. Bras. Climatol.* **2016**, *19*. [CrossRef]
62. Emiliano, V.M.; de Lima, N.G.B.; Baratto, J.; Galvani, E. Variabilidade pluviométrica na área paulista da bacia hidrográfica do rio Ribeira de Iguape (Brasil) e a influência do ENOS, a partir da técnica box-plot. *Terr. Plur.* **2024**, *18*, e2423128. [CrossRef]
63. Barreiro, M. Influence of ENSO and the South Atlantic Ocean on climate predictability over southeastern South America. *Clim. Dyn.* **2010**, *35*, 1493–1508. [CrossRef]
64. Correa, M.G.G. Correlação entre o Índice de Oscilação Sul (IOS), precipitação pluviométrica e vazão fluvial na bacia hidrográfica do rio Piquiri-PR durante o fenômeno ENOS (1997–1999). In Proceedings of the XI Encontro Nacional da ANPEGE, Presidente Prudente, Brazil, 9–12 October 2015; pp. 7553–7563.
65. Guimarães Correa, M.G.; Galvani, E. O impacto do ENOS na variabilidade temporal da precipitação pluviométrica na bacia hidrográfica do rio Piquiri-PR. *Rev. Inst. Geol.* **2021**, *41*, 21–33. [CrossRef]
66. Alves De Oliveira, T.; Miguel De Bodas Terassi, P.; Galvani, E. Correlação entre o fenômeno ENOS e a precipitação na bacia hidrográfica do rio Pomba-MG/RJ. In Proceedings of the XV ENANPEGE; Palmas, Tocantins, Brazil, 9–13 October 2023.
67. Pierri Daunt, A.B.; Sanna Freire Silva, T. Beyond the park and city dichotomy: Land use and land cover change in the northern coast of São Paulo (Brazil). *Landsc. Urban Plan.* **2019**, *189*, 352–361. [CrossRef]
68. Dias, R.L.; de Oliveira, R.C. Caracterização socioeconômica e mapeamento do uso e ocupação da terra litoral sul do estado de São Paulo. *Soc. Nat.* **2015**, *27*, 111–123. [CrossRef]
69. Miyao, S.Y.; Harari, J. Estudo preliminar da maré e das correntes de maré da região estuarina de Cananéia (25os-48ow). *Bol. Inst. Oceanogr.* **1989**, *37*, 107–123. [CrossRef]
70. Cheliz, P.M.; De Oliveira, R.C. Geomorfologia e estrutura superficial da paisagem de zonas costeiras rochosas: Um estudo de caso na ilha do Cardoso (litoral sul de São Paulo). *Rev. Bras. Geogr. Fis.* **2021**, *14*, 3667–3694. [CrossRef]
71. de Bodas Terassi, P.M.; Baratto, J.; Oscar-Júnior, A.C.d.S.; Galvani, E.; Sobral, B.S.; de Gois, G.; de Oliveira, T.A.; Biffi, V.H.R. Trends and shifts of climate extremes in eastern Paraná state, Brazil. *Theor. Appl. Climatol.* **2024**, *155*, 6863–6886. [CrossRef]
72. Varuolo-Clarke, A.M.; Smerdon, J.E.; Williams, A.P.; Seager, R. Gross discrepancies between observed and simulated twentieth-to-twenty-first-century precipitation trends in southeastern South America. *J. Clim.* **2021**, *34*, 6441–6457. [CrossRef]
73. Varuolo-Clarke, A.M.; Williams, A.P.; Smerdon, J.E.; Ting, M.; Bishop, D.A. Influence of the South American low-level jet on the austral summer precipitation trend in southeastern South America. *Geophys. Res. Lett.* **2022**, *49*, e2021GL096409. [CrossRef]
74. Regoto, P.; Dereczynski, C.; Chou, S.C.; Bazzanela, A.C. Observed changes in air temperature and precipitation extremes over Brazil. *Int. J. Climatol.* **2021**, *41*, 5125–5142. [CrossRef]
75. Hernández Ayala, J.J.; Palance, M. Exploring trends in Earth's precipitation using satellite-gauge estimates from NASA's GPM-IMERG. *Earth* **2025**, *6*, 130. [CrossRef]
76. Monteiro, C.A.F. *A Dinâmica Climática e as Chuvas no Estado de São Paulo: Estudo Geográfico Sob Forma de Atlas*; IGEOG/USP: São Paulo, Brazil, 1973.
77. de Bodas Terassi, P.M.; Galvani, E.; Steinke, V.A.; da Silva, C.A. Identification of homogeneous rainfall regions in the eastern watersheds of the state of Paraná, Brazil. *Climate* **2017**, *5*, 53. [CrossRef]
78. Córdova, M.; Célleri, R.; van Delden, A. Dynamics of precipitation anomalies in tropical South America. *Atmosphere* **2022**, *13*, 972. [CrossRef]
79. Almagro, A.; Meira Neto, A.A.; Vergopolan, N.; Roy, T.; Troch, P.A.; Oliveira, P.T.S. The drivers of hydrologic behavior in Brazil: Insights from a catchment classification. *Water Resour. Res.* **2024**, *60*, e2024WR037212. [CrossRef]

80. Ballarin, A.S.; Sousa Mota Uchôa, J.G.; dos Santos, M.S.; Almagro, A.; Miranda, I.P.; da Silva, P.G.C.; da Silva, G.J.; Gomes Júnior, M.N.; Wendland, E.; Oliveira, P.T.S. Brazilian water security threatened by climate change and human behavior. *Water Resour. Res.* **2023**, *59*, e2023WR034914. [CrossRef]
81. de Alvarenga, C.M.; Alvarenga, L.A.; Melo, P.A.; Tomasella, J.; Pinto, P.R.F.; de Mello, C.R.; Isidoro, J.M.G.P. Impacts of climate change on the hydrology of a highly disturbed tropical river basin. *Earth* **2026**, *7*, 52. [CrossRef]
82. Gomes, L.C.; Bianchi, F.J.J.A.; Cardoso, I.M.; Schulte, R.P.O.; Fernandes, R.B.A.; Fernandes-Filho, E.I. Disentangling the historic and future impacts of land use changes and climate variability on the hydrology of a mountain region in Brazil. *J. Hydrol.* **2021**, *594*, 125650. [CrossRef]
83. Wasko, C.; Nathan, R.; Stein, L.; O'Shea, D. Evidence of shorter more extreme rainfalls and increased flood variability under climate change. *J. Hydrol.* **2021**, *603*, 126994. [CrossRef]
84. Chen, Y.; Guan, Y.; Shao, G.; Zhang, D. Investigating trends in streamflow and precipitation in Huangfuchuan basin with wavelet analysis and the Mann-Kendall test. *Water* **2016**, *8*, 77. [CrossRef]
85. Filho, A.O.S.; Kalinowski, L.M. Transposição e hidrelétricas: O desconhecido Vale do Ribeira (PR-SP). *Estud. Av.* **2012**, *26*, 269–286. [CrossRef]
86. Companhia Brasileira de Alumínio (CBA). Energia: Ativos de Geração de Energia Renovável, Complexo Juquiá. Available online: https://www.cba.com.br/energia/ (accessed on 21 October 2026).
87. Chong, X.Y.; Vericat, D.; Batalla, R.J.; Teo, F.Y.; Lee, K.S.P.; Gibbins, C.N. A review of the impacts of dams on the hydromorphology of tropical rivers. *Sci. Total Environ.* **2021**, *794*, 148686. [CrossRef]
88. Chaudhari, S.; Pokhrel, Y. Alteration of river flow and flood dynamics by existing and planned hydropower dams in the Amazon river basin. *Water Resour. Res.* **2022**, *58*, e2021WR030555. [CrossRef]
89. Costa, D.d.A.; Bayissa, Y.; Villas-Boas, M.D.; Maskey, S.; Lugon Junior, J.; da Silva Neto, A.J.; Srinivasan, R. Water availability and extreme events under climate change scenarios in an experimental watershed of the Brazilian Atlantic Forest. *Sci. Total Environ.* **2024**, *946*, 174417. [CrossRef]
90. SIGRH. Sistema Produtor São Lourenço Tem Nova Vazão Outorgada. 23 June 2016. Available online: https://www.sigrh.sp.gov.br/pageitems/450/news/1510 (accessed on 29 October 2026).
91. Companhia de Saneamento Básico do Estado de São Paulo (Sabesp). Boletim dos Mananciais, 11 April 2019: Operação do Sistema São Lourenço em 2018. Available online: https://www.sabesp.com.br/site/uploads/file/boletim/2019/boletim%20mananciais_11abr19.pdf (accessed on 29 October 2026).
92. Maciel, A.L.; Alves, D.; Sant'Anna, S. Análise dos processos de desmatamento e regeneração nas unidades de conservação pertencentes no Vale do Ribeira (SP/PR) por meio de classificações de imagens de sensoriamento remoto. *Rev. Bras. Cartogr.* **2021**, *73*, 261–277. [CrossRef]
93. Rosa, M.R.; Brancalion, P.H.S.; Crouzeilles, R.; Tambosi, L.R.; Piffer, P.R.; Lenti, F.E.B.; Hirota, M.; Santiami, E.; Metzger, J.P. Hidden destruction of older forests threatens Brazil's Atlantic Forest and challenges restoration programs. *Sci. Adv.* **2021**, *7*, eabc4547. [CrossRef]
94. Caballero, C.B.; Ruhoff, A.; Biggs, T. Land use and land cover changes and their impacts on surface-atmosphere interactions in Brazil: A systematic review. *Sci. Total Environ.* **2022**, *808*, 152134. [CrossRef]
95. Lopes, B.S.; Corrêa, K.A.B.; Ogasawara, M.E.K.; Precinoto, R.S.; Cassiano, C.C.; Sell, B.M.; Melo, R.S.; dos Reis Oliveira, P.C.; Ferraz, S.F.d.B. How does land use cover change affect hydrological response in the Atlantic Forest? Implications for ecological restoration. *Front. Water* **2022**, *4*, 998349. [CrossRef]
96. Rigala, A.; Sibanda, M.; Dube, T. Delineation of floodplain wetland extent and land use/land cover changes in the UMngeni catchment (2000–2024) using Landsat data. *Earth* **2026**, *7*, 95. [CrossRef]
97. Kayitesi, N.M.; Guzha, A.C.; Mariethoz, G. Impacts of land use land cover change and climate change on river hydro-morphology-a review of research studies in tropical regions. *J. Hydrol.* **2022**, *615*, 128702. [CrossRef]
98. Possantti, I.; Barbedo, R.; Kronbauer, M.; Collischonn, W.; Marques, G. A comprehensive strategy for modeling watershed restoration priority areas under epistemic uncertainty: A case study in the Atlantic Forest, Brazil. *J. Hydrol.* **2023**, *617*, 129003. [CrossRef]
99. Viana, J.F.d.S.; Montenegro, S.M.G.L.; Srinivasan, R.; Santos, C.A.G.; Mishra, M.; Kalumba, A.M.; da Silva, R.M. Land use and land cover trends and their impact on streamflow and sediment yield in a humid basin of Brazil's Atlantic Forest biome. *Diversity* **2023**, *15*, 1220. [CrossRef]
100. Atwood, A.; Coe, M.T.; Neill, C.; Maracahipes-Santos, L.; Brando, P.; Riskin, S.H.; Castanho, A.; Deegan, L.; Silveiro, A.C.; Macedo, M.N. Deep soil water reservoirs modulate land use and drought effects on the water budget of Amazon headwaters. *Water Resour. Res.* **2025**, *61*, e2024WR039729. [CrossRef]
101. Barati, A.A.; Zhoolideh, M.; Azadi, H.; Lee, J.H.; Scheffran, J. Interactions of land-use cover and climate change at global level: How to mitigate the environmental risks and warming effects. *Ecol. Indic.* **2023**, *146*, 109829. [CrossRef]

102. Agência Nacional de Energia Elétrica (ANEEL). SIGA—Sistema de Informações de Geração da ANEEL. Available online: https://dadosabertos.aneel.gov.br/dataset/siga-sistema-de-informacoes-de-geracao-da-aneel (accessed on 29 October 2026).
103. Companhia de Saneamento Básico do Estado de São Paulo (Sabesp). Relatório de Sustentabilidade 2018. Available online: https://www.sabesp.com.br/site/uploads/file/relatorios_sustentabilidade/sabesp_rs_2018_portugues%281%29.pdf (accessed on 29 October 2026).
104. Copernicus, D.E.M. GLO-90 Digital Elevation Model. Available online: https://registry.opendata.aws/copernicus-dem/ (accessed on 29 October 2026).

Disclaimer/Publisher's Note: The statements, opinions and data contained in all publications are solely those of the individual author(s) and contributor(s) and not of MDPI and/or the editor(s). MDPI and/or the editor(s) disclaim responsibility for any injury to people or property resulting from any ideas, methods, instructions or products referred to in the content.